uc3m | Universidad Carlos III de Madrid

Bachelor Thesis

Degree in Aerospace Engineering

2018 - 2019

Automatization of a Flame Propagation Experimental Setup using LabVIEW

Alexis Jesús Lora de la Calle

SUPERVISED BY:

Fernando Veiga López

June, 2019

ABSTRACT

The present dissertation aims at automating the propagation of a premixed flame in a quasi-bidimensional geometry using as a combustion chamber a Hele-Shaw cell. This project is carried out by the Thermal and Fluids Engineering Department of Universidad Carlos III de Madrid.

The work done explained in this document includes the synchronization of a high-speed camera recording the flame front as it advances through the cell (at a rate of 1000 frames per second), with a DAQ charge amplifier which collects pressure and acceleration signals provided by sensors distributed along the cell domain, with the objective of relating each pair of data with a real image so as to characterize the flame. Also, the control of all the gases participating in the experiment (methane is used as fuel, and air as oxidant), as well as the mechanisms used to ignite the mixture are incorporated. Finally, the process by which the pneumatic actuators open and close both ends of the combustion chamber has been achieved to be automatic. All this automatization is accomplished using the software LabVIEW.

Lastly, a verification of the program is presented where three different cases (with different equivalent ratios) are analyzed and compared with previous studies, providing as a result the right functioning of the code and thus, its validation. For this task, a MatLab code is needed to undertake the image processing procedure in order to convert the pictures taken by the camera into useful data employed for the calculation of the flame front velocity.

Keywords: Automation, Hele-Shaw cell, Premixed flame, LabVIEW, Instabilities.

ACKNOWLEDGEMENTS

First of all, I would like to thank Fernando Veiga for giving me the opportunity to participate in such a cool experiment. Working with him during these months has been a real pleasure because of the closeness with which he has treated me and the patience and kindness he has had with me at all times.

This project could not have been done without the support of my whole family, and especially my mother's, who always listens to me, stays by my side and encourages me in everything I do regardless of my hard character with her; and my grandma's, who despite not knowing what this project is about, is the engine of the whole family and an example of strength and willpower.

I want to give my most special thanks to Ger, who has been there everyday to bear with all the details of this project and my life in general, guilty of making me that happy.

Of course, my friends deserve a special mention, who have always been there in my best moments, but also in my worst ones and have believed in me even though I am not sure they understand what I am studying.

And last but not least, I would like to thank Dani who has helped me from the very first day and without whom I would still be lost in the first course.

Contents

List of Figures

List of Tables

List of Symbols

α	Thermal diffusivity
β	Zel'dovich number
δ_L	Flame thickness
ℓ°	Characteristic thickness
μ	Viscosity coefficient
ν	Kinematic viscosity
$\overline{\overline{\tau}}'$	Stress tensor
Φ	Viscous dissipation rate
ϕ	Equivalence ratio
ρ	Density
τ_L	Reaction time
τ_{ij}	Shear stress
$\overrightarrow{f_{m_i}}$	Volumetric forces acting on species i
$\vec{q}$	Heat flux
c	Concentration
c_p	Specific heat capacity at constant pressure
$D_{i,j}$	Mass diffusion coefficient of species i in species j
e	Internal specific energy
E_a	Activation energy
h	Specific enthalpy
J_i	Mass diffusion flux of species i
k	Thermal conductivity
L	Characteristic Length
Le	Lewis number
m_i	Mass of species i
p	Pressure
Pr	Prandtl number
q	Specific heat transfer

Q_c	Rate of heat release due to chemical reaction
Q_r	Rate of heat release due to radiation
R	Ideal gas constant
Re	Reynolds number
S_L	Laminar flame speed
Sc	Schmidt number
T	Temperature
t	Time
T_{ad}	Adiabatic flame temperature
U	Characteristic Velocity
u	Velocity
V	Velocity
v	Specific volume
w_i	Net rate of production/consumption of species i per unit volume
w_v	Specific work due to volumetric changes
Y_i	Mass fraction of species i

1 Introduction

Automation has a long history that goes back more than 5000 years. Since the dawn of time, mankind has researched how to save human energy and perform their daily activities with the help of utensils, tools and machinery [1].

Already in Ancient Greece the first mechanisms appeared whose movement was achieved through hydraulic devices, pulleys and levers. An example of this is Heron of Alexandria, who invented the first automatic door by making use of water vapour. Even so, it was not until 1760 with the Industrial Revolution when people realized how important automatization was since it allowed the production without the human intervention, leading in this way to a reduction in lead times and thus, in costs.

Thenceforth, with the development and birth of new technologies such as microelectronics, computers and more recently, Internet, men and women have been able to create processes more refined and improved than ever. Thanks to that, the majority of simple, repetitive or delicate tasks of any field can now be performed by machines. However, automation is in continuous improvement and innovation, and very soon artificial intelligence will go beyond the actual limits and will be capable of carrying out any type of activity (learning from experience) without the need of any supervision.

Although the process of automatization is the core of this project, another key aspect such as combustion cannot be forgotten. The combustion process is probably, of all the chemical processes, the most important one, as the current civilization is based on it. One of the fundamental difference between civilized and primitive man is precisely the consumption of energy.

With the passage of time, the source of energy employed for different activities has evolved a lot. Examples of that could be wood, water, coal, petroleum and its derivatives, light or nuclear fission. Nevertheless, since the late 20^{th} century, the concern about pollution, climate change and the scarcity of fossil resources is redirecting the efforts towards the production of renewable energies (e.g., solar, wind, biomass...) as they are characterized by having low emissions and can be naturally replenished on a human timescale.

Therefore, with the idea of adapting to the new age and leaving behind the oil and all the non-renewable energies that pollute a lot, it has been decided to use methane (CH_4) for this project. This gas, although one may think that belongs to the non-renewable group as it is a hydrocarbon, in reality it can be considered renewable because it is obtained from urban waste and human and animal excrements, and it can be replaced quickly, as opposed to petrol, for example, that is limited [2].

Nonetheless, other gases such as Dimethyl Ether (DME) or Hydrogen (H_2) are typically used in this experiment too due to their characteristics, efficiency and cleanliness, among others.

1.1 Socio-Economic and environmental impact

As part of the motivation for performing the automation of such an experiment, it is of interest to consider its socio-economic impact.

A better understanding of the physics behind the premixed flames will help to increase engine efficiency by improving its chamber design, and consequently this will lead to a reduction in the amount of needed fuel which in turn will bring a decrease in the pollutants generated.

Another interesting aspect of this investigation is related to the rapid development of small scale technologies, microelectronic and portable electronic devices whose energy requirements are increasingly higher. This has brought back the interest on Micro Power Generation Systems (MPGS) of high energy density since present batteries do not satisfy such a demanding level [3]. This undoubtedly asks for a research in micro combustion which must be carried out in a cell as the one presented in this report (a Hele-Shaw cell) in order to satisfy the social demands.

Regarding the environmental impact, the improvement of combustion, as it has just been said, translates into a considerable minimization of very harmful pollutants like CO or NOx.

Methane on its behalf, coming from the decomposition of organic waste, defecation of animals and the anaerobic putrefaction of plants [2], it is noxious and indeed it is considered a greenhouse gas, which means that its presence in the atmosphere affects the temperature and the Earth's climate system [4].

However, its combustion capacity is very high. Thereby, by using it as a combustible instead of letting it climb to the atmosphere, on the one hand all those dangerous emissions can be avoided, and on the other hand, a cheap, effective and unlimited supply is guaranteed, contributing in this manner to a more sustainable waste management, and to the energy independence from other producing countries.

1.2 Objectives

In the frame of this context, the ambition of this project is to help in the work carried out at the Thermal and Fluids Engineering department of Universidad Carlos III de Madrid, by automating the process in which a premixed flame propagates in

a quasi-2D channel. In this case, a Hele-Shaw cell will be used as a combustion chamber to perform the experiment.

The software used for that purpose will be LabVIEW, a system-design platform and development environment from National Instruments that uses a visual programming language.

More specifically, the aim of this report is to synchronize two software which are essential for the study and understanding of the flames: a high-speed camera (Memrecam HX3) in charge of taking pictures at a rate of 1000 frames per second, and a DAQ, a charge amplifier which will catch and record the signal recovered by the pressure sensors and accelerometer distributed along the cell.

With that, it will be possible to relate each pair of pressure data recorded at a specific instant with an image showing the appearance of the flame at that same moment. This necessity arises since at the point in which the report is started there is a time delay between both that does not provide accurate results as a consequence of the use of different drivers for each device.

1.3 Regulatory framework

As the experiment setup is based on the combustion of a flammable gas, in this case methane, some security and prevention measures must be applied.

This prevention list has been studied and done by the University. The student has signed a risk contract adapted to the specific labour developed in the laboratory written by his supervisor and revised by the University.

As methane belongs to the first group of gases (flammable, not corrosive and low toxicity gases), several points need to be taken into consideration:

- Control of the pressure and the mass flow of the gas from the source.
- Perform the experiment and store the fuel in an isolated location away from heat and light.
- Forbiden ignitable devices or materials.
- In the case of gas leak, it is important to close the valves and ventilate, without using electrical devices.
- Absolutely forbidden to touch the experiment when the flame is ignited due to the high temperature.
- Prepare an emergency plan for fire extinction and disposing of extinguisher.

Also, as the student has worked with pneumatic actuators being able to press down up to 100 kg each, some extra rules have been accepted and signed such as not touching the actuators while they are being calibrated and stay at least one meter far from it to avoid entrapment and cuts.

As a final remark, it must be considered that all the automatization process has been developed under the LabVIEW standard programming language, while all data post-processing have been regulated under the MatLab standard programming. Since they are commercial software, their licenses need to be purchased (for the case of MatLab, an academic version has been used).

2 Combustion

Combustion, commonly referred to as burning, is a complex sequence of chemical exothermic reactions (i.e., energy is released) between any combustible material (fuel) and an oxidizer to produce heat and light, among others. "It is interdisciplinary in nature, comprising thermodynamics, chemical kinetics, fluid mechanics and transport phenomena" [5].

Depending on the kind of combustion, carbon dioxide, water, and other elements can also be obtained as products. The typical reaction for the combustion of methane [6], the gas used in this experiment, is presented below in (2.1).

$$CH_4 + 2O_2 \rightarrow aCO_2 + bH_2O + cCH_4 + dH_2 + eO_2 + fH + gO + hCO + ... \quad (2.1)$$

where the lower case letters a-h represent the unknown stoichiometric coefficients of the various product species listed.

This equation is known as the main reaction since it represents the products in their most stable state and consequently, it is used as a basis for all the calculations. To satisfy this condition, the reaction has to come to the point of chemical equilibrium, defined as the instant at which forward and reverse reactions occur at exactly the same rate (assuming no outside influence due to temperature changes, mechanical work interactions or outside heat transfer).

Note that even though it is not represented in (2.1), secondary reactions (dissociation/recombination reactions) are also taking place during the course of the combustion process and hence, they cannot be forgotten. Also, as the experiment is carried out with the oxygen from the air ($21\%O_2 + 79\%N_2$), nitrogen should also be taken into consideration.

2.1 Types of combustion

As the field of combustion is so vast and a lot of factors come into play, multiple possibilities arise and several classifications of fundamental combustion phenomena can be distinguished:

2.1.1 Complete and incomplete combustion

Complete combustion, also called "Clean Combustion", happens when there is sufficient oxidant so that all carbon and hydrogen atoms from the fuel molecules combine with oxygen atoms to form only two products: carbon dioxide and water.

Thus, equation (2.1) can be simplified to obtain:

$$CH_4 + 2O_2 \rightarrow CO_2 + 2H_2O \tag{2.2}$$

As explained above, nitrogen is going to play a role as well in the reaction since methane is reacting with air, so the right form of (2.2) applied to the case of interest should be the following:

$$CH_4 + 2(3.76N_2 + O_2) \rightarrow CO_2 + 2H_2O + 7.52N_2 \tag{2.3}$$

Complete combustion is a more efficient process for generating heat since all the fuel is being consumed. It is called stoichiometric combustion [5], and it takes place when the concentration ratio of the reactants reaches the unity, that is, when the equivalence ratio, ϕ, is equal to 1.

The equivalence ratio measures the extent to which the reactants deviate from the stoichiometric condition, and it is defined in (2.4) as the fuel-to-oxidizer ratio in the actual fuel-air mixture (F/O) divided by that of a stoichiometric mixture:

$$\phi = \frac{(F/O)}{(F/O)_{st}} = \frac{Y_{CH_4}/Y_{O_2}}{(Y_{CH_4}/Y_{O_2})_{st}} \tag{2.4}$$

where the subscript "st" designates the stoichiometric state and $Y_i = m_i/m_{total}$ represents the mass fraction of species i.

A combustion process can be classified attending to the values of this ratio into:

- **Fuel-Lean** ($\phi < 1$): characterized by having a proportion of oxygen higher than the one needed, appearing then O_2 as part of the products.
- **Stoichiometric** ($\phi = 1$)
- **Fuel-Rich** ($\phi > 1$): characterized by having a proportion of fuel higher than the portion needed. In this case, some unburnt fuel may appear again as a product.

Therefore, if a reaction has not enough oxygen or fuel, incomplete combustion develops. Particularly, the fuel-rich kind is often undesirable because it releases less energy than complete combustion (as not all the fuel is consumed) and produces toxic substances such as carbon monoxide (CO) and soot [7].

As a final remark, a bright orange flame is typically produced during this process [8] whereas a blue one is originated throughout the complete combustion.

2.1.2 Premixed versus Non-premixed combustion

One of the most important classification of combustion phenomena makes a difference between premixed and non-premixed flames. This separation depends on whether the reactants, fuel and oxidant, are mixed before the chemical reaction takes place or not.

- **Premixed flames**: The reactants are already well mixed before reaction is initiated. As it can be seen in Figure 2.1a, the colour of the flame is typically blue-green due to the chemiluminescence of some excited radicals (C_2 and CH) [9, 10].

  This is the case for a Bunsen burner, in which fuel and air are mixed within the tube, and the gas is ignited downstream. A premixed flame front will propagate until it finds its steady state position in the form of the well-known Bunsen cone [11]. This premixed flame phenomenon will be explained in more detail in Section 3, as it is the case of interest in this report.

- **Non-Premixed flames**: Both fuel and oxidizer arrive to the combustion chamber from different sides. They receive the name of "diffusion flames" due to the fact that reactants are brought together through the molecular process of diffusion. These flames radiate in a bright yellow-orange color as it can be observed in Figure 2.1b caused by the radiation of soot particles which dominate over the blue chemiluminescence, also present at the base of it. As diffusion is slower than combustion, this flames tend to burn slower than the previous one.

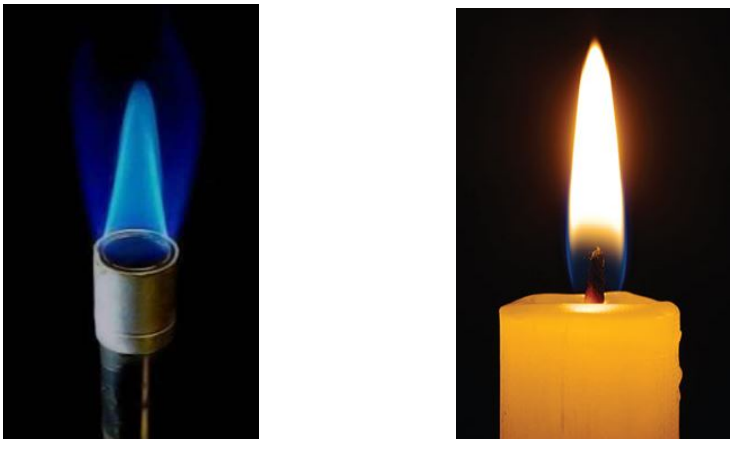

(a) (b)

Figure 2.1: Different types of flames: **(a)** premixed flame obtained with a Bunsen burner [12], **(b)** non-premixed flame of a candle [13].

2.1.3 Laminar versus Turbulent combustion

Based on the behaviour of the flow, flames can also be distinguished into two types: laminar or turbulent. This can be done by calculating the Reynolds number, Re, defined as the ratio of inertial forces to viscous forces within a fluid:

$$Re = \frac{UL}{\nu} \tag{2.5}$$

where U is the characteristic velocity of the fluid, L is the characteristic dimension of the geometry and ν is the kinematic viscosity (defined as the ratio of dynamic viscosity to density).

When Re is small, approximately $Re < 2300$, the flow experiments a laminar regime; the viscous forces are dominant and the fluid particles travel smoothly. This type of flames has an orderly behaviour (see Figure 2.2a) which allows them to be analyzed with patterns.

When Re > 4000, flames tend to be turbulent. Inertial forces now dominate over the viscous ones. The fluid flows faster, and thus mixing and transport are enhanced. However, turbulent regime is characterized by rapid, random and nonuniform fluctuations of the flow velocity (see Figure 2.2b) [5], complicating its characterization.

(a) (b)

Figure 2.2: Comparison of **(a)** diffusion laminar flame (ethylene) [14], and **(b)** diffusion turbulent flame [15].

In this particular case, the focus of the project will be put on laminar premixed flames.

2.2 Transport phenomena

When the molecules in any region of a fluid medium have an excess of energy, concentration, or momentum, the system will try to restore the balance by transporting the proper property from the areas in which the levels are high to the deficient regions [5].

This event can be perfectly understood with the schematic shown in Figure 2.3 representing diffusion of heat, mass and viscous motion, respectively, being all of them key to describe the propagation of flames. The three properties depicted are temperature (T), concentration (c) and velocity (V). In all the three cases diffusion occurs from A to B due to the magnitude difference between them (being such of A greater than the one of B). The main reason for this behaviour can be found in the continuous collision between the fluid molecules (in constant random motion), that will attempt to even out the macroscopic non-uniformities.

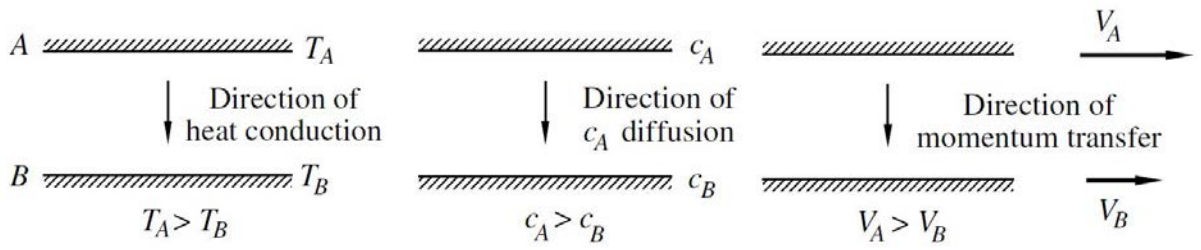

(a) Heat Conduction (b) Mass Diffusion (c) Momentum Transfer

Figure 2.3: Schematic of heat, mass and momentum diffusion [5].

The rate at which diffusional transport happens depends on the property gradients and diffusion coefficients, which can be explained by the following laws:

2.2.1 Fourier's law

"The heat flux between two bodies resulting from thermal conduction is proportional to the magnitude of the temperature gradient between them and opposite to it in sign." [16]

$$\vec{q} = -k\nabla T \tag{2.6}$$

where q is the heat flux, k is the thermal conductivity coefficient of the medium and ∇T represents the (negative) gradient of temperature in the direction of the heat flow (i.e., conduction occurs in the direction of decreasing temperature).

Associated with this thermal conduction process, the characteristic spreading rate

is defined in (2.7) as the *thermal diffusivity*:

$$\alpha = \frac{k}{c_p \rho} \tag{2.7}$$

where ρ is the density and c_p the specific heat capacity at constant pressure.

2.2.2 Fick's law

"Diffusion occurs in response to a concentration gradient expressed as the change in concentration due to a change in position." [17]

$$\vec{J_i} = -\rho D_{i,j} \nabla Y_i \tag{2.8}$$

where $\vec{J_i}$ is the mass diffusion flux of species i and $D_{i,j}$ is the mass diffusion coefficient of species i in species j.

2.2.3 Newton's law

"The rate of momentum transfer per unit area between two adjacent layers of fluid is proportional to the negative value of the velocity gradient between them." [18]

$$\tau_{ij} = -\mu \nabla u \tag{2.9}$$

where τ_{ij} is the momentum flux or shear stress, μ is the viscosity coefficient and u is the velocity.

2.2.4 Dimensionless numbers

In order to compare and establish the relative importance of each transport phenomenon in the analysis of the system, it is convenient to define some dimensionless numbers [5] that will help in next sections to predict different behaviours of the flame.

- **Schmidt number:** it measures the relative influence of viscosity to mass diffusion.

$$Sc_{i,j} = \frac{\mu}{\rho D_{i,j}} \tag{2.10}$$

- **Prandtl number:** it compares the relative influence of viscosity to thermal diffusion.

$$Pr = \frac{\mu c_p}{k} \tag{2.11}$$

- **Lewis number:** it contrasts the relative influence of thermal to mass diffusion.

$$Le_i = \frac{\alpha}{D_{i,j}} = \frac{Sc_{i,j}}{Pr} = \frac{k}{c_p \rho D_{i,j}} \tag{2.12}$$

Usually, the Lewis number to be used is the one of the limiting reactant depending on whether the flame is rich or lean. However, there is an improved and more accurate version of this number, defined as the effective Lewis number L_{eff}, introduced by Joulin and Mitani [19], which basically controls the development of the hydrodynamic instabilities due to diffusion effects [20] and diffusive thermal instabilities [21] (to be explained later in Section 3.4).

These numbers are different for lean and rich flames, respectively shown in (2.13):

$$Le_{eff} = \frac{Le_O + (1 - \beta(\phi - 1))Le_F}{2 - \beta(\phi - 1)} \quad Le_{eff} = \frac{Le_F + (1 + \beta(\phi - 1))Le_O}{2 + \beta(\phi - 1)} \tag{2.13}$$

where the subscripts O and F respectively refer to oxidizer and fuel, and β for the Zel'dovich number, a dimensionless number which provides a quantitative measure for the activation energy (E_a) of a chemical reaction [22].

The values of different effective Lewis numbers as a function of the equivalence ratio can be consulted in Table 1. This values together with the adiabatic flame temperature (T_b) will be useful in later sections.

Table 1: Properties of methane-air mixture calculated at room temperature (T_u = 298.15 K) [20].

ϕ	T_b [K]	Le_F	Le_O	Le_{eff}	β
0.70	1833.71	0.98	1.10	1.01	7.26
0.80	1992.31	0.98	1.10	**1.02**	6.78
0.90	2130.22	0.98	1.10	1.03	6.42
1.00	2222.16	0.98	1.08	**1.03**	6.19
1.10	2206.32	0.98	1.08	1.04	6.23
1.20	2132.02	0.98	1.09	**1.06**	6.41

2.3 Conservation equations

To have a better understanding of premixed-flame propagation, it is necessary to state the main conservation laws that define the dynamics and thermodynamics of a chemically reacting flow. These equations are the conservation laws of mass,

momentum, energy and the concentration of the individual species [23].

- **Mass conservation:** In a chemical reaction it can be stated that the sum of the mass of reactants must be equal to the sum of the mass of the products.

$$\frac{\partial \rho}{\partial t} + \nabla \cdot (\rho \vec{u}) = 0 \tag{2.14}$$

where t is the time.

- **Continuity of species:** It appears when reacting flows are present. It establishes that the increase of the total mass of species i depends on the velocity at which it diffuses in the medium together with the velocity at which it is produced [24]. Mathematically it can be expressed as:

$$\rho \frac{\partial Y_i}{\partial t} + \nabla \cdot (\rho \vec{u_i} Y_i) = w_i + \nabla \cdot \vec{J_i}, \qquad i = 1, ..., k \tag{2.15}$$

where w_i is the net rate of production/consumption of species i per unit volume and the term $\rho Y_i \vec{u_i}$ accounts for the convective transfer.

- **Momentum conservation:** The Newton's second law of motion, when applied to a moving fluid element, states that the force acting on a system is equal to the rate of change of its momentum. This force is due to the pressure and the shear-normal stress distributions acting on the surface (i.e., surface forces) and the mass forces (i.e., volumetric forces) [25].

$$\rho \left(\frac{\partial \vec{u}}{\partial t} + \vec{u} \cdot \nabla \vec{u} \right) = -\nabla p + \nabla \cdot \overline{\overline{\tau}}' + \rho \sum_{i=1}^{N} Y_i \overrightarrow{f_{m_i}} \tag{2.16}$$

where p is the pressure, $\overline{\overline{\tau}}'$ is the stress tensor, N is the number of species and $\overrightarrow{f_{m_i}}$ the volumetric forces acting on species i.

- **Energy conservation:** The first law of thermodynamics (2.18) states that the total energy of a system is neither created nor destroyed, only transformed, and therefore it must be conserved.

$$\frac{\partial}{\partial t} \left(e + \frac{u^2}{2} \right) \rho + \vec{u} \cdot \nabla \left(e + \frac{u^2}{2} \right) \rho = -\nabla \cdot (p \vec{u}) + \Phi - \nabla \cdot \vec{q} + \rho \sum_{i=1}^{N} Y_i \overrightarrow{f_{m_i}} \cdot \vec{u} + Q_r + Q_c \tag{2.17}$$

where e is the internal specific energy, Q_r and Q_c represent, respectively, the

rates of heat release due to radiation and chemical reaction, and $\Phi = \overline{\overline{\tau}}' : \nabla \vec{u}$ states for the viscous dissipation rate.

2.4 Adiabatic flame temperature

The adiabatic flame temperature (T_{ad}) is one of the most important parameters when studying combustion reactions. It can be defined as the temperature reached by the product mixture assuming an isobaric process at pressure p and adiabatic conditions—i.e., no heat transfer outside of the system ($\delta Q = 0$).

This temperature provides a very useful upper bound for several applications since any heat losses in the system will lead to a reduction in temperature as compared to the adiabatic limit [6]. Thereby, one can estimate the losses of the system by contrasting the actual temperature against the adiabatic one.

For its calculation, using the fist principle of thermodynamics and assuming mass is conserved (closed system):

$$\delta q = de + \delta w_v \tag{2.18}$$

where δq is the specific heat transfer from the surroundings, de is the change of specific internal energy and δw_v is the specific work due to volumetric changes ($\delta w_v = pdv$). Note that e is a property of the system, and hence, de an exact differential of the process (only initial and final state matters), whereas δq and δw_v are path-dependent quantities [5].

Equation (2.18) can also be written as:

$$\delta q + \delta w_R = de + pdv = dh - vdp \tag{2.19}$$

where $v = 1/\rho$ is the specific volume, δw_R is the frictional work and h is the specific enthalpy, which is related to the specific inner energy e by:

$$h = e + \frac{p}{\rho} \tag{2.20}$$

Assuming the system is adiabatic ($\delta q = 0$) at constant pressure ($dp = 0$) and neglecting the work done by friction ($\delta w_R = 0$), making use of (2.19) one can obtain that the variation of specific enthalpy is zero ($dh = 0$). Therefore integrating:

$$h_2 - h_1 = 0 \tag{2.21}$$

where subscript “1” refers to the reactants and “2” to the products.

Figure 2.4 shows that the enthalpy is indeed conserved and also describes the reaction process: it starts first at a temperature T_1 and then it changes to T^0, moment at which the chemical reaction takes place consuming the reactants and the heat is released. This amount of heat is then used to warm up the products to the final temperature $T_2 = T_{ad}$ [5].

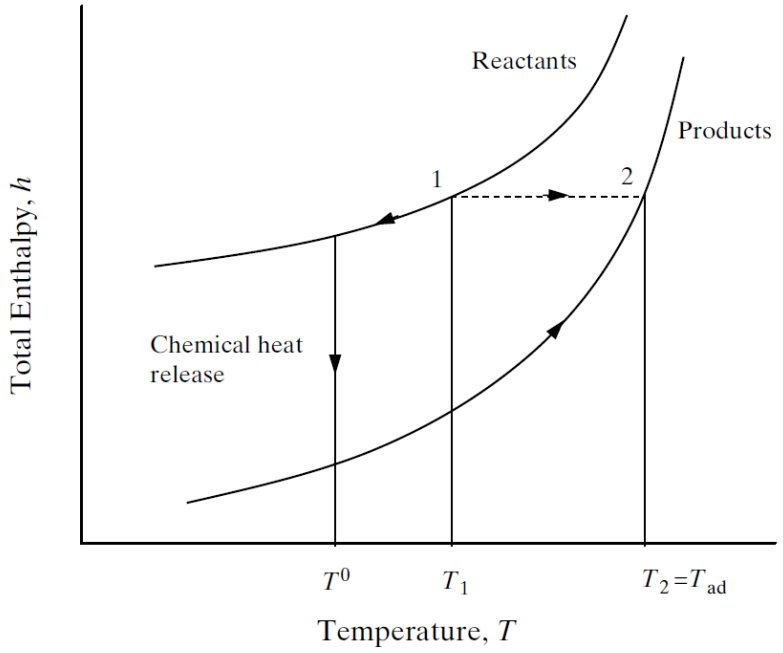

Figure 2.4: Enthalpy-Temperature diagram illustrating the adiabatic flame temperature and the principle of energy conservation [5].

The enthalpy can also be defined as a function of the enthalpy of formation (Δh_f^o) and sensible enthalpy (last term on the RHS of (2.22)):

$$h_1 = h_2 = h = \sum_{i=1}^{N} Y_i \left(\Delta h_{f_i}^o(T_{ref}) + \int_{T_{ref}}^{T} c_{p_i}(T) dT \right) \tag{2.22}$$

where $\Delta h_{f_i}^o(T_{ref})$ is the reference enthalpy at the reference temperature T_{ref}. This temperature may be arbitrarily chosen, but most frequently $T_{ref} = 298.15K$ is used [11].

Using tables 2 and 3 for h_i^o and $c_{p_i}(T)$ respectively, together with (2.21) and (2.22), one will be able to obtain the adiabatic flame temperature of the mixture in the case of complete combustion. If the reaction is incomplete, the mass fractions of the products will be unknown (since the stoichiometric coefficients are unknown as well), and the problem will become more complex (out of the scope of this report).

Table 2: Molecular weight (MW), enthalpy of formation (Δh_f^o) and specific heat at constant pressure (c_p), at 1 atm and 298.15 K [6].

Substance	Formula (state)	MW	Δh_f^o kJ/mol	c_p J/(mol K)
Methane	CH_4 (g)	16.04	-74.87	35.64
Nitrogen	N_2 (g)	28.01	0	29.07
Oxygen	O_2 (g)	31.99	0	29.32
Carbon Dioxide	CO_2 (g)	44.01	-393.55	37.20
Water	H_2O (g)	18.02	-241.85	33.45

Table 3: Specific heat at constant pressure as a function of temperature ($c_p(T)$) measured in J/(mol K) [6].

Substance	Formula	$c_p(T) = a + b(T/1000) + c(T/1000)^2 + d(T/1000)^3$				
	(state)	a	b	c	d	Range, K
Methane	CH_4 (g)	19.887	50.242	12.686	-11.011	273-1470
Nitrogen	N_2 (g)	27.336	6.230	-0.9508	0	273-3770
Oxygen	O_2 (g)	28.186	6.301	-0.7499	0	273-3770
Carbon Dioxide	CO_2 (g)	*	*	*	*	273-3770
Water	H_2O (g)	29.182	14.503	-2.0235	0	273-3770

*$c_{p_{CO_2}} = 75.153 - 0.18732 \cdot 10^{-3}T - 661.85T^{-\frac{1}{2}}$

3 Laminar Premixed Flames

As explained in Section 2.1.2, one of the differences between non-premixed and premixed flames is that the former will situate itself between the fuel and oxidizer whereas the latter will tend to propagate and consume the unburnt mixture, that is, the premixed flames can be categorized as a wave phenomenon [5].

When this event manifests in a duct with the inlet and outlet boundaries situated far enough from the wave front, it can be treated as a simplified 1D front [26] as shown in Figure 3.1. Here, a flame-stationary frame is assumed and hence, the upstream unburnt mixture approaches the flame front with velocity u_u and temperature T_u, leaving it with velocity u_b and temperature T_b.

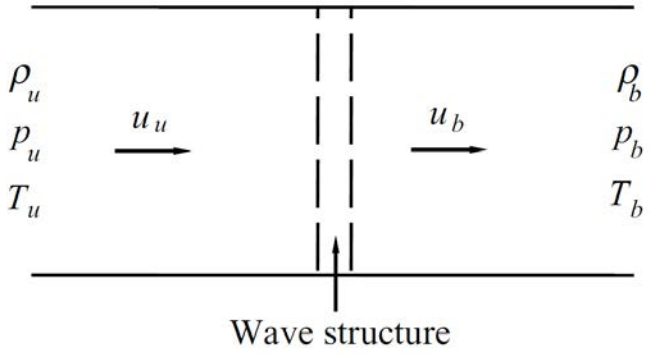

Figure 3.1: Schematic of 1-D combustion wave in a premixture [5].

Consequently, the model used for this study will be based on the following conservation equations derived from (2.14), (2.15), (2.16) and (2.17) respectively, assuming plane, steady, one-dimensional flow:

Mass:

$$\rho_u u_u = \rho_b u_b \tag{3.1}$$

Species:

$$\rho_u u_u Y_u = -w_b \tag{3.2}$$

Momentum:

$$\rho_u u_u^2 + p_u = \rho_b u_b^2 + p_b \tag{3.3}$$

Energy:

$$h_u + \frac{1}{2}u_u^2 + q = h_b + \frac{1}{2}u_b^2 \tag{3.4}$$

where the subscripts u and b account respectively for the unburnt and burnt state far upstream and downstream of the wave.

Once defined the fundamental equations, the next point will be to describe the flame structure (Section 3.1) and the main aspects that affect it as a function of the equivalence ratio: the adiabatic flame temperature (Section 3.2) and the laminar flame speed (Section 3.3). Finally, the different types of flame instabilities that can be found in a propagating wave will be analyzed (Section 3.4).

3.1 Flame structure

Considering the mixture of interest is enough off-stoichiometric such that the concentration Y of the limiting reactant governs the reaction, then a one-reactant reaction model can be used ($Reactant \rightarrow Products$) [5].

As the deficient reactant is totally consumed upon crossing the flame, initially the concentration of the fresh mixture can be interpreted by Y_u, and after crossing the wave front it will suffer a decrease down to $Y_b = 0$, as presented in Figure 3.2. Conversely, the temperature will experience the opposite: it will start with a low one (typically ambient temperature), T_u, to finally increase up to T_b, commonly referred to as adiabatic temperature (see Section 3.2).

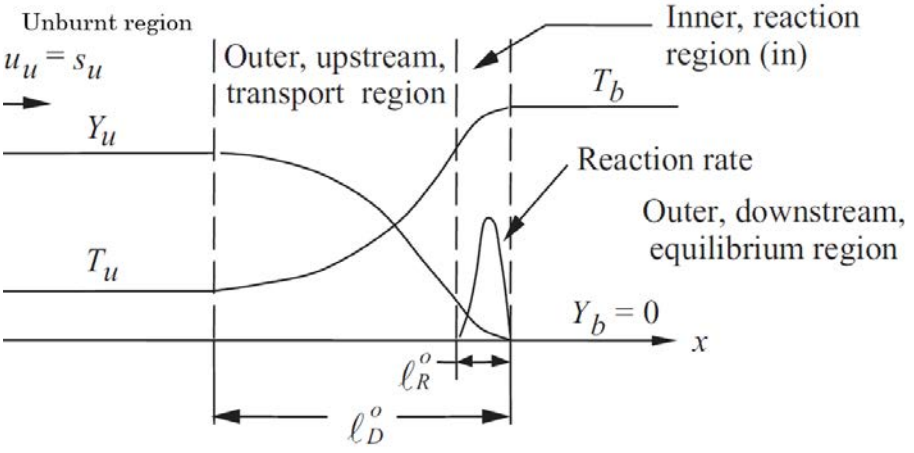

Figure 3.2: Schematic of the premixed flame structure [5].

Figure 3.2 also shows all the regions or stages through which the combustion goes on. The first one is situated on the left hand side and it can be denoted as unburnt region since the reaction has not begun yet. Next to it, the preheat or transport region is placed, of characteristic thickness ℓ_D° and governed by heat and mass diffusion. Here, as the mixture comes closer to the flame, the temperature increases until T_b is reached whereas Y decreases as it is consumed. This continuous heating leads to the mixture ignition, represented at the reaction region (right to the preheat region), of characteristic thickness $\ell_R^\circ \ll \ell_D^\circ$, where diffusive transport has a greater influence than convective transport. This zone is characterized by

being a source of heat and a sink for the reactant. Finally, at the right hand side of Figure 3.2, the burnt or equilibrium section is found where products develop.

"The flame structure can therefore be considered to consist of two distinct zones, namely the preheat zone in which convection and diffusion dominate and balance, and the reaction zone in which reaction and diffusion balance" [5].

3.2 Adiabatic flame temperature of a premixed flame

For the case of interest, the adiabatic flame temperature can be derived from energy and species conservation across the flame, and assuming constant c_p and $Y_b = 0$ as the limiting reactant is totally consumed.

Imposing upstream and downstream boundary conditions; $x = -\infty$ corresponds to the initial unburnt state and $x = \infty$ represents the burnt gases at equilibrium, it can be obtained:

$$c_p(T_b - T_u) = qY_u \tag{3.5}$$

From this equation (3.5) it can be extracted that the heat released from the reaction is used to heat the fresh mixture [5]. Therefore, the downstream temperature T_b is just the adiabatic flame temperature T_{ad}, given by:

$$T_b = T_{ad} = T_u + \frac{qY_u}{c_p} \tag{3.6}$$

Once defined the procedure to obtain the adiabatic flame temperature, it is convenient to comment the factors that have some influence on it. As Chung K.Law [5] comments, these factors are: the fuel concentration, the fuel type and the pressure of the fuel–air mixture.

The latter in this case is not going to be relevant since as the combustion chamber is always open either at one side or the other (to be explained in Section 4.3), the chamber pressure will be that of the ambient with little changes throughout the experiment.

Nonetheless, the fuel concentration, or in other words, the equivalence ratio, will indeed affect T_{ad} as it can be extracted from Figure 3.3. A general trend can be observed for all the compounds represented including methane: peaking around $\phi = 1$ (vertical dash line), thus decreasing as the mixture becomes either leaner or richer. This is reasonable because of the need to heat up the excess reactants for off-stoichiometric conditions [5].

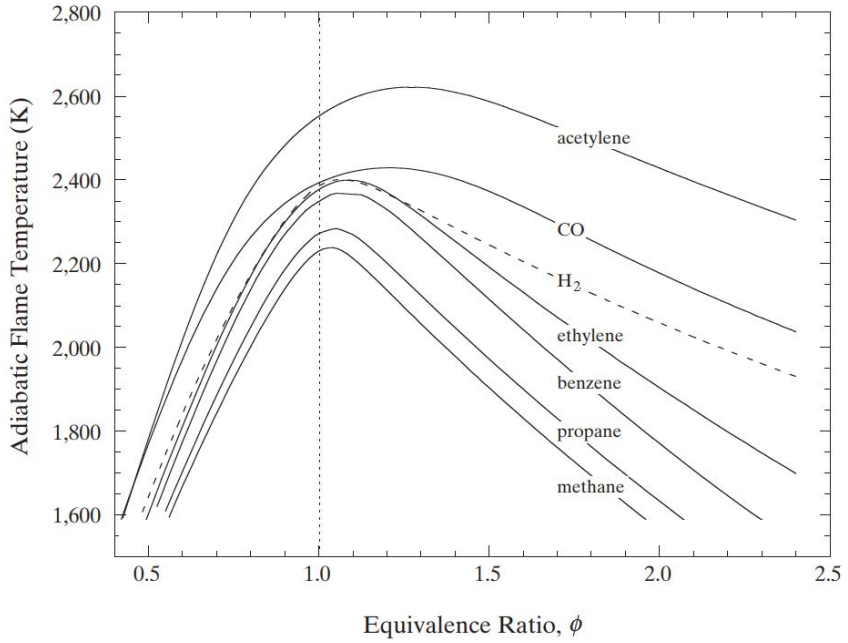

Figure 3.3: Adiabatic flame temperature as a function of equivalence ratio for several fuel–air mixtures [5].

The last important ingredient affecting T_{ad} is the fuel type or the C/H ratio. If this ratio increases, the adiabatic flame temperature increases as well. One of the reasons that explains this phenomenon is that usually containing large C/H ratios comprises having more double and triple bonds of carbon, which are able to contain a larger potential energy than single bonds [5]. This behaviour can be ratified in Figure 3.3 as acetylene (with a triple bond) has a higher T_{ad} than, for example, methane (formed by single bonds).

3.3 Laminar flame speed

Assuming the convention used in Figure 3.1, the laminar burning speed, S_L or U_L, is the velocity with which the fresh mixture approaches the flame (perpendicularly to it). There are several methods for its determination experimentally, such as the Bunsen flame method, the Flat and One-Dimensional flame methods, the Outwardly propagating spherical flame method, the Stagnation flame method, by numerical computation or using profile-based determination [5].

Analytically, the laminar flame speed can be calculated, as the adiabatic flame temperature, from the energy and species conservation equations. Imposing the same boundary conditions as before, and after some algebra, the following formula

is achieved [27]:

$$S_L = \frac{\rho_b}{\rho_u}\sqrt{\frac{\alpha_b}{\tau_L}} \tag{3.7}$$

where $\tau_L = (\beta^2/2)\tau_c \exp(E_a/RT_b)$ represents the reaction time, τ_c the elastic collision time, R the ideal gas constant ($R = 8.314$ JK^{-}1mol^{-}1) and $\delta_L \equiv S_L\tau_L$ the flame thickness.

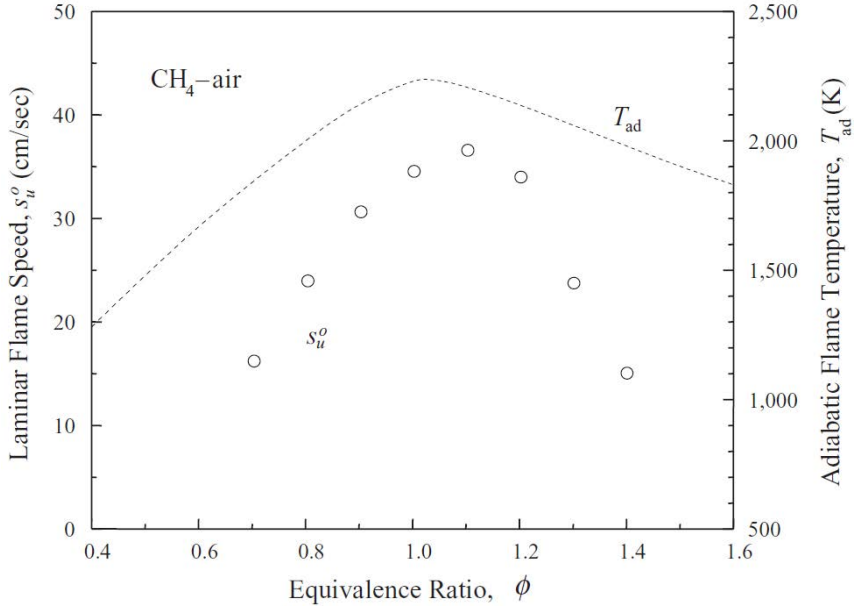

Figure 3.4: Adiabatic flame temperatures and laminar flame speeds of atmospheric methane-air mixtures as a function of equivalence ratio [5].

As Figure 3.4 shows, the laminar flame speed follows a similar trend and shape as T_{ad}: it becomes maximum at $\phi \approx 1.1$ and decreases for both leaner and richer mixtures within a range between 0.15 and 0.35 m/s.

This only reaffirms the strong dependence of S_L on the adiabatic flame temperature as fuels with larger heat of combustion and hence, with larger T_{ad}, tend to propagate faster as they are more excited

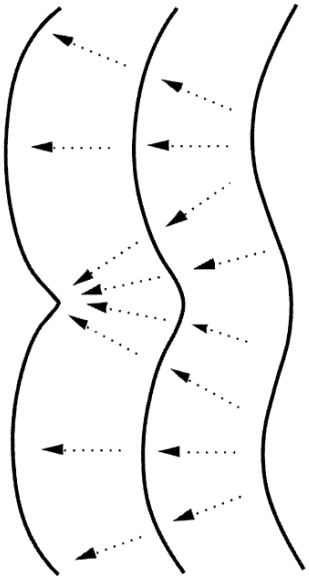

Figure 3.5: Wrinkled flame front due to instabilities [28].

However, there is one last thing to take into account that affects this velocity and it is not included in Figure 3.4: the wrinkled front caused by instabilities that increases the flame surface area and thus propagation speeds (see Figure 3.5). This will be explained in more detail in the next section (Section 3.4).

3.4 Flame Instabilities

The study of premixed flames presented in previous sections is limited to some hypothesis (plane steady one-dimensional flow, negligible viscous and friction forces, adiabatic process...) that are useful to understand the basic properties and parameters that govern this type of flames. However, the flame front is not typically that perfect and planar as shown in Figure 3.1. In fact, characterizations of flame propagation are always oversimplified because planar flame fronts are unstable per se [29]. In reality, flame fronts are curved, commonly denoted as wrinkled flame fronts, as depicted in Figure 3.5, which have an impact in their development and evolution across the cell.

Among the instabilities described in [21] for a similar experiment in a Hele-Shaw cell, the only ones taking part in this project and therefore the ones to be considered are the hydrodynamic (Darrieus-Landau), the thermo-diffusive and the thermoacoustic instabilities. The first two are intrinsic instabilities of flame fronts (although the second one depends on the Lewis number) whereas the third one is usually generated by an unsteady flame propagating in a cavity [29].

There are two more types not considered here due to the characteristics of the

experiment: the Rayleigh-Taylor (RT) instability, caused by buoyant convection (destabilizing for upward-propagating flames since the lower-density fluid lies underneath the higher-density fluid, and stabilizing for downward-propagating flames); and the Saffman-Taylor (ST) instability, due to the viscosity change across the flame front (destabilizing when a less-viscous fluid displaces a more viscous fluid) [21].

3.4.1 Darrieus-Landau (DL)

The Darrieus-Landau instabilities, are mainly caused by the density variation across the flame front between the fresh mixture (higher density) and the burnt gases which are at a higher temperature (lower density). As this difference in temperature and density is always present because the density of the resulting products is less than that of the reactants ($\rho_b/\rho_u \approx T_u/T_b \ll 1$), this effect occurs essentially in all cases.

Basically, the main consequence of DL instabilities is the deviation of the streamlines in such a way that it favours further wrinkling of the flame, modifying in this way both the upstream and downstream flow field over a distance of the order of the wavelength of wrinkling [29, 30].

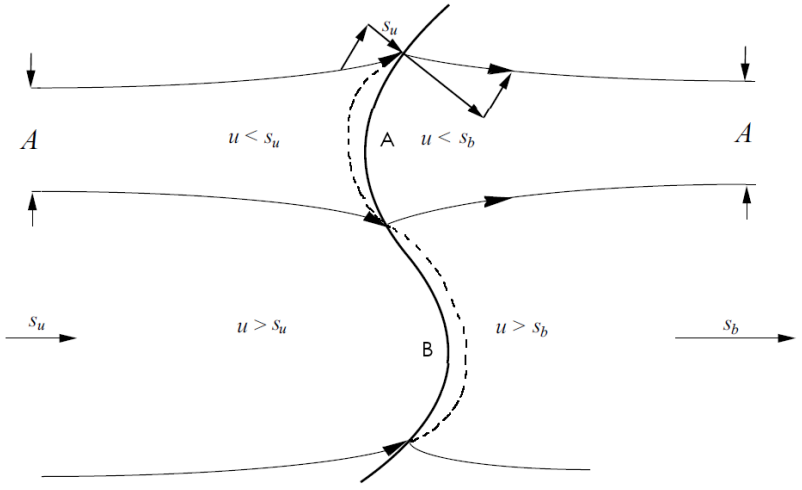

Figure 3.6: Schematic of the development of hydrodynamic instabilities [31].

This behaviour can be observed in Figure 3.6. Assuming a constant flame speed s_u and knowing that far upstream and downstream the front the velocity perturbations vanish, the areas (A) of the streamtubes should remain the same there [5, 29]. Also, as the normal component of the burnt mixture velocity at the surface is larger than that of the fresh mixture due to thermal expansion ($s_b = s_u\rho_u/\rho_b$, being $\rho_u/\rho_b \gg 1$), and assuming equal tangential components, it is clear that the streamlines must diverge and converge respectively when approaching the convex and concave segments

of the flame. A direct consequence of this, is that the flow velocity at point 'A' (convex segment) slows down due to the widening of the streamtube. Since S_u wants to be maintained, and the local velocities of the approaching flow can no longer balance each other, this segment of the flame front must move into the unburnt mixture, therefore progressing with respect to the flow at point 'A'. By analogy, the same phenomenon happens with the concave segment, showing how the flow at point 'B' will further recede into the burned mixture.

Hence, Darrieus-Landau instabilities tend to increase the amplitude of wrinkling and amplify the initial deformation, growing faster those disturbances of short wavelengths as long as they are not comparable to the flame thickness [32]. Nonetheless, this effect can be stabilized by diffusion processes within the flame that may overcome the destabilizing effect of thermal expansion.

3.4.2 Diffusive-thermal (DT)

The diffusive-thermal instabilities may occur independently of hydrodynamic effects. They are the outcome of the competition between the molecular diffusion of species and the conduction of heat. In other words, they are produced when thermal and molecular diffusion coefficients are unequal, that is, when the Lewis number of the limiting reactant is different than unity [21].

The diffusive-thermal instability can stabilize or destabilize more the Darrieus-Landau instability depending on the Lewis number.

(a) (b)

Figure 3.7: Propane flames at the same propagation speed but with different equivalence ratio: **(a)** Lean flame and **(b)** rich flame [29].

For a $Le > 1$ flame, the heat diffusion predominates over the mass diffusion and hence, the burning is intensified at the concave segments and weakened at the convex ones. Consequently, its direct effect is the smoothing of the wrinkles and thus, the stabilization of the front. Such a flame is known as a cellular stable flame [5] and it can be seen in Figure 3.7a and at the left hand side of Figure 3.8 respectively in a real simulation and in a schematic way.

Conversely, for a $Le < 1$ flame, mass diffusion is enhanced and therefore, a cellular unstable flame is developed as the wrinkling is increased. As it is shown in the right image of Figure 3.8, burning velocity is intensified at the convex part and weakened at the concave segment, contributing in this way to the destabilization of the wave front, which can be better understood with Figure 3.7b where the flame is presented with many cells of smaller size (cusps) as compared to Figure 3.7a, deeper aspect ratio and having an overall chaotic aspect [29].

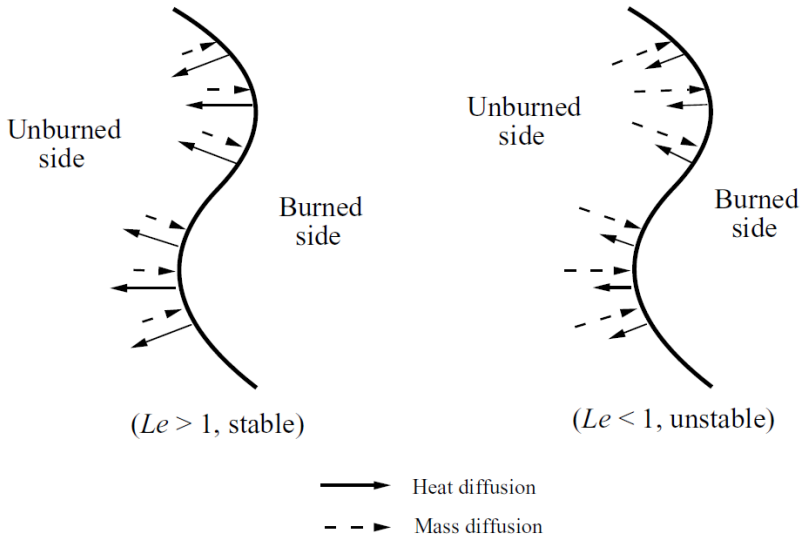

Figure 3.8: Schematic of the development of diffusive-thermal cellular instabilities [5].

However, it must be taken into account that cellular flames are typically observed in rich mixtures of heavy hydrocarbon fuels, as in the case of propane (Figure 3.7b), whereas for light fuels, such as hydrogen, this behaviour is observed in lean mixtures rather than in rich ones [29].

For the case studied, the methane Lewis number is around 1, so this kind of instability will not be of high importance. Nonetheless, it is convenient to take it into consideration since more gases are usually employed in this experiment (propane, nitrogen, dimethyl ether, helium...), whose Le is different than 1 and thus, the effect of these diffusive-thermal instabilities is observable.

3.4.3 Thermo-acoustic

Thermo-acoustic instabilities are typical of flames propagating in confined spaces such as gas turbines, rocket engines or cells. They can be very dangerous since a small amount of chemical energy of combustion is enough to produce huge damages when transformed into mechanical energy [29].

The reason why these instabilities occur is because flames can spontaneously produce acoustic oscillations (studied first in tubes by Mallard and Le Chatelier [33]) if the laminar flame velocity is approximately above 16 cm/s [27]. After arriving to the walls and coming back, there might be a coupling between these acoustic waves and the flame front, appearing in this way the cited instabilities. Thus, the behaviour of the flame will change according to the frequency and amplitude of the wave, being more aggressive the higher the laminar flame speed is.

There are many possible coupling mechanisms but in this report only two will be analyzed: pressure and acceleration coupling.

The pressure coupling is considered the simplest mechanism [29] as the temperature of the gas is changed due to adiabatic compression, which in turn causes the change in the heat release rate, modifying thereby directly the velocity of the flow. This usually happens when the flame velocity oscillates between 16 and 25 cm/s and it is known as the primary thermo-acoustic instability.

The second coupling mechanism, the acceleration one, modulates the surface area of the wrinkled flame front by the periodic acceleration of the acoustic wave. This inevitably leads to the modulation of the global heat release rate and again, to the change in the flame speed. This is typical of flame velocities exceeding 25 cm/s.

Figures 3.9 and 3.10 represent the development of a rich propane flame propagating across the Hele-Shaw cell from two different points of view. Here it can be clearly seen the cited perturbations.

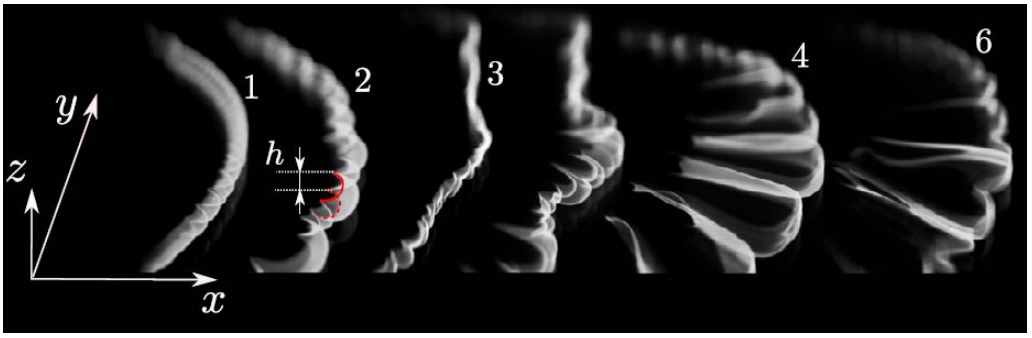

Figure 3.9: Side view of the flame front propagating across the cell (gas used: propane at $\phi = 1.1$) [20].

On the one hand, stage 3 represents the direct consequence of the first instability: the flattening of the wave front. As this first coupling mechanism is not so strong, the interaction between the acoustic wave and the flame is able to stabilize the latter.

On the contrary, when the second instability also comes into play, its produces the development of finger-like shape adopted by the wave front as presented in stage 4.

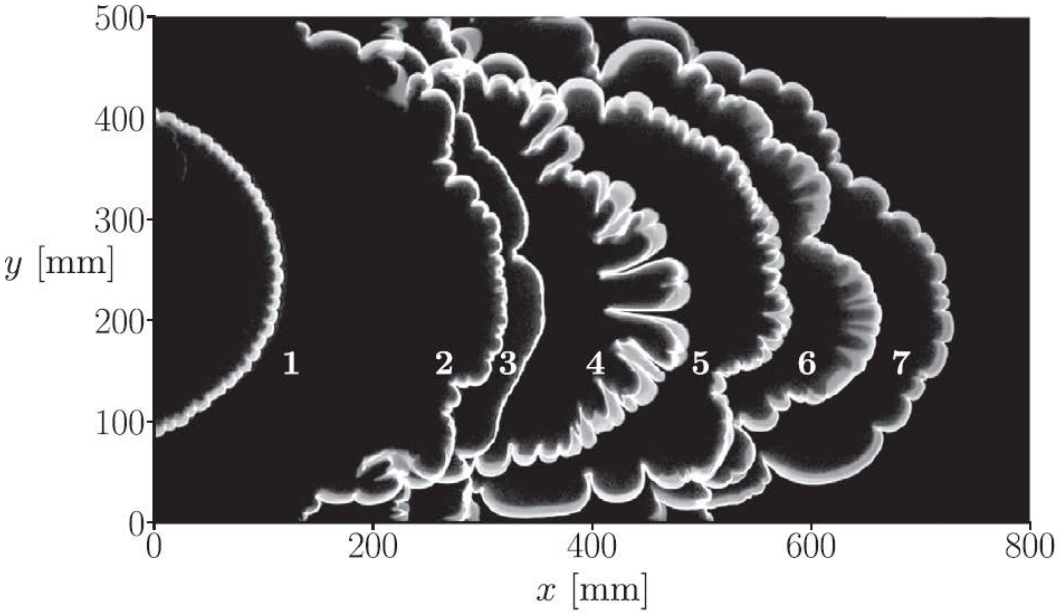

Figure 3.10: Top view of the flame front propagating across the cell (gas used: propane at $\phi = 1.1$) [20].

Also in these figures it can be seen how the cusps originated by the Darrieus-Landau and the diffusive-thermal instabilities at stage 1 develop and grow due to the acoustic coupling until they reach the cited finger-shaped structure at stage 5.

4 Experimental setup and procedure

This section is aimed at defining and explaining the function of the main devices that compose the experimental setup as well as the procedure followed in each ignition. Also, the main changes that has undergone the cell during the last year will be treated.

4.1 Experimental setup

The workplace where the student has spent most of his time, together with all the elements used for the proper development of the experiment can be seen in Figure 4.1.

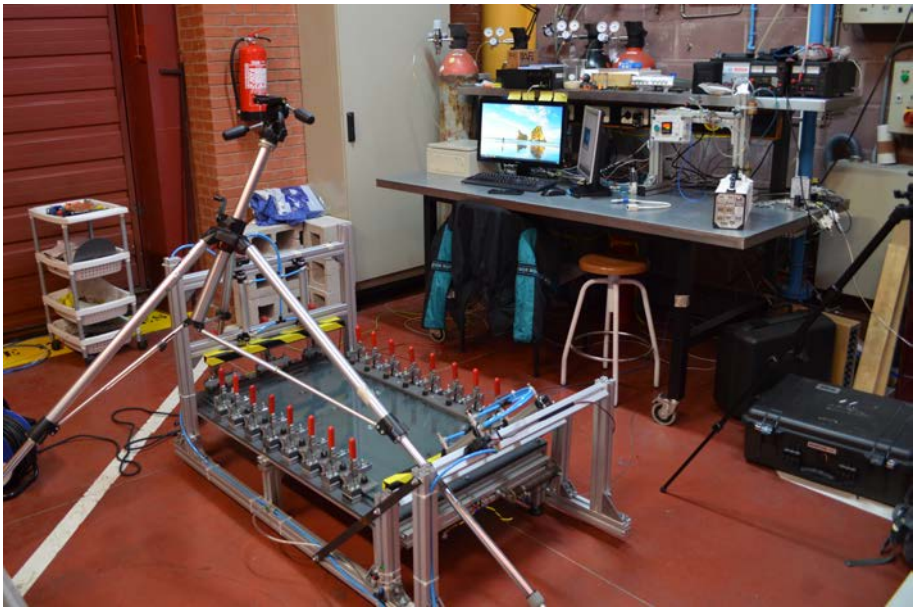

Figure 4.1: Workplace and experimental setup.

To begin with, the Hele-Shaw cell (key part of this project) will be presented. This construction, fabricated by the fluid mechanics group here at Universidad Carlos III de Madrid, will be used as a combustion chamber, therefore holding the whole reaction process. It is characterized by having a 2-dimensional domain as the length and width are much larger than the height (L x $H \gg h$) [21].

Figure 4.2 represents schematically the design of this cell. It basically consists of two parallel flat plates separated by an infinitesimally narrow gap, enclosing a maximum volume of L x H x h = 90 x 50 x 1 cm^3 [20]. Nevertheless, the actual observed area is a little bit smaller since the important length is the one from the glow plug to the opposite end of the chamber (80 cm).

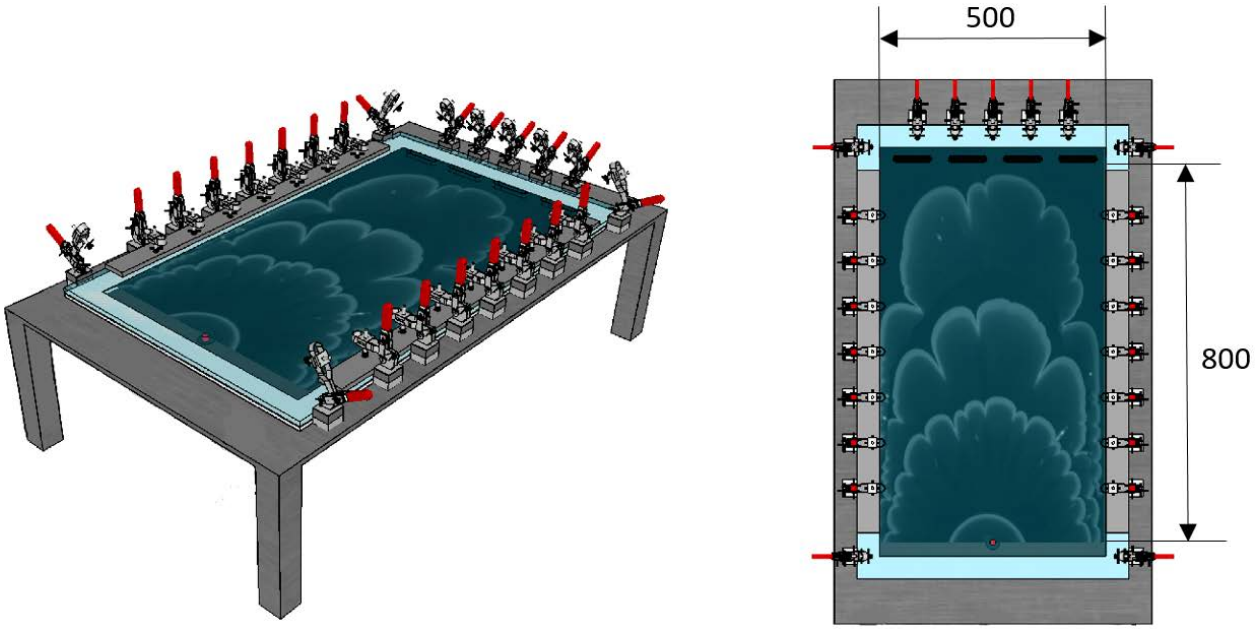

Figure 4.2: Representation of the Hele-Shaw cell (units in mm) [34].

A more detailed view is presented in Figure 4.3, where all the main components can be identified.

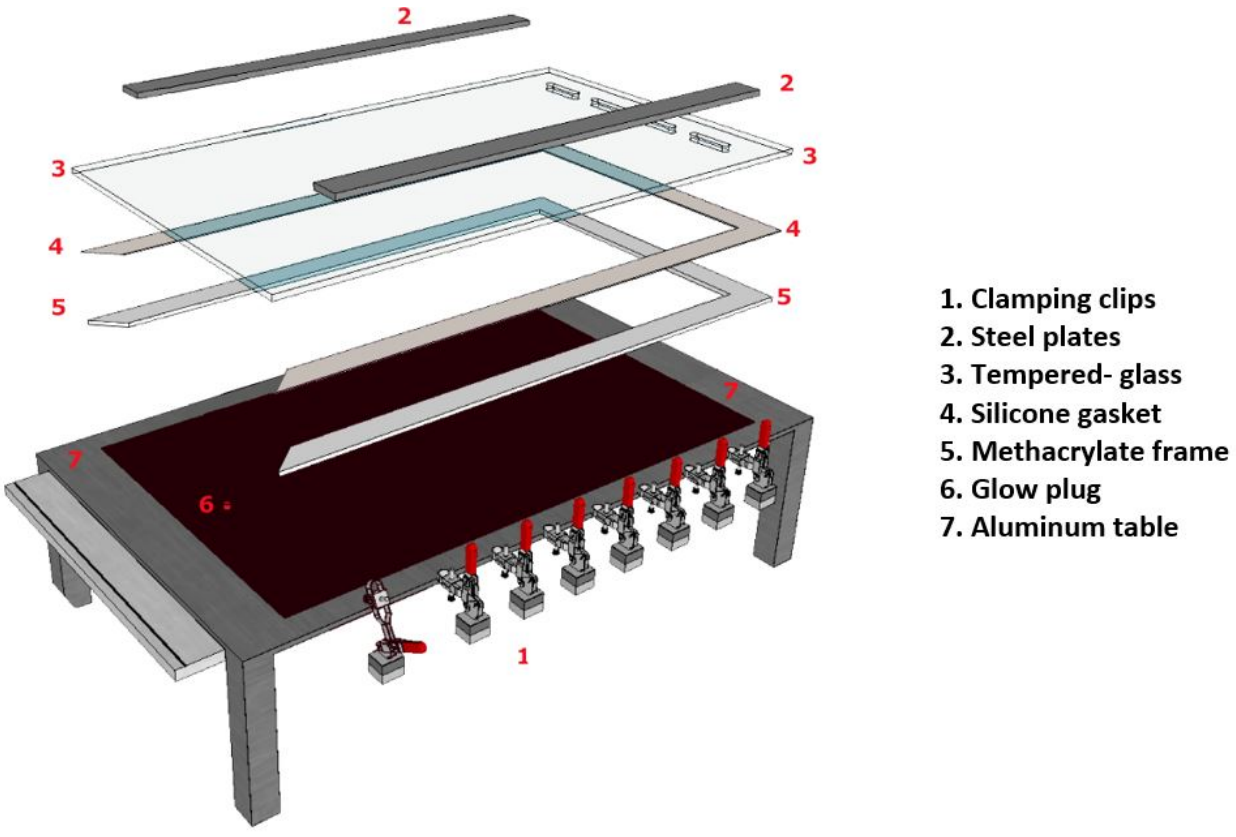

Figure 4.3: Exploded view of the Hele-Shaw cell [34].

The top cover (3) is a tempered-glass plate whose transparency enables the observation of the flames in the cell while the lower one (7) is a rigid aluminum table that gives structural strength and support to the rest of the components. Also, in order to prevent leaks, a silicone gasket (4) is used to seal the cell.

The methacrylate frame (5) defines the space where the combustion is generated, and if the height of the combustion chamber needs to be changed, it can be done by stacking 3 mm-thick PVC laminae inside the hollow frame [20]. All these elements are attached to the table by means of steel plates (2) that distribute the force done by the clamping clips (1).

Finally, the glow plug (6), used for the ignition of the flame. This device (see Figure 4.4a) is typically employed to aid starting diesel engines. It consists of a metal cylinder with a high resistance in an extreme that produces heat when the current passes through it [35]. This glow plug is connected to a battery that generates a voltage of 12 V_{DC} (Figure 4.4b) and to a switch (Figure 4.4c) that activates the circuit for certain time (prefixed by the user) thus igniting the flame.

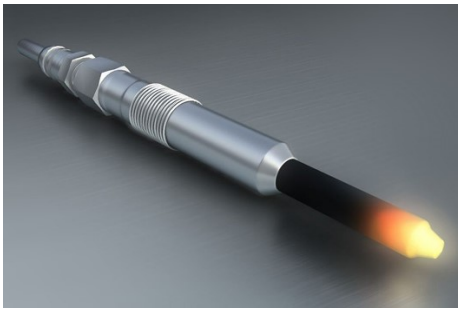

(a) Bosh Duraspeed glow plug [36]

(b) Battery

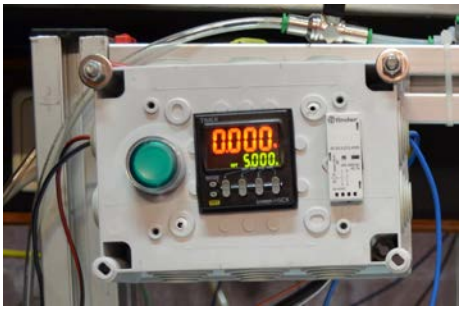

(c) Switch

Figure 4.4: Devices used for the flame ignition.

Although not depicted in Figure 4.3, there are four more elements present in the Hele-Shaw cell: two pneumatic actuators ("Actuator 1" at the left or ignition end, "Actuator 2" at the right side of the cell), represented in Figures 4.5 and 4.6, which open or close both sides of the combustion chamber as needed (each being able to

press down up to 100 kg); two pressure sensors distributed along the domain to measure the acoustic vibrations at different locations (see Figure 4.5); an accelerometer in the middle to capture the vertical displacements provoked by the compressed gas (see Figure 4.5); and four small injection ports (Figure 4.7) through which the chamber is filled with the fuel-air mixture.

Note that in Figure 4.5 it may seem that more than 2 pressure sensors appear, but in reality they are plugs with the same shape drilled with the aim of being able to change the position of these devices in case it is wanted to study the pressure at a different point (see Figure 4.7).

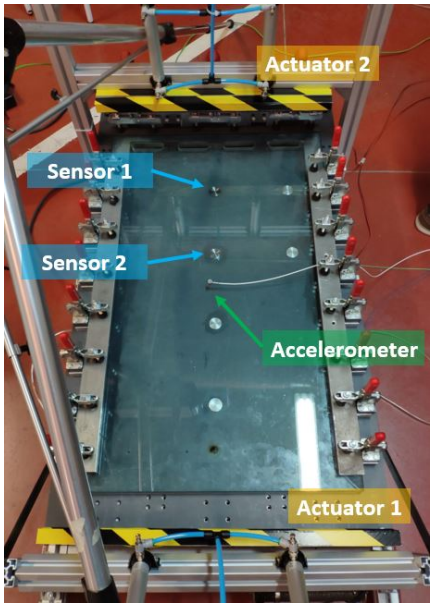

Figure 4.5: Hele-Shaw cell.

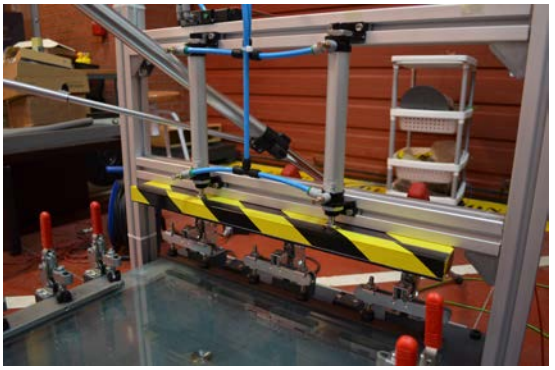

Figure 4.6: Actuator 2.

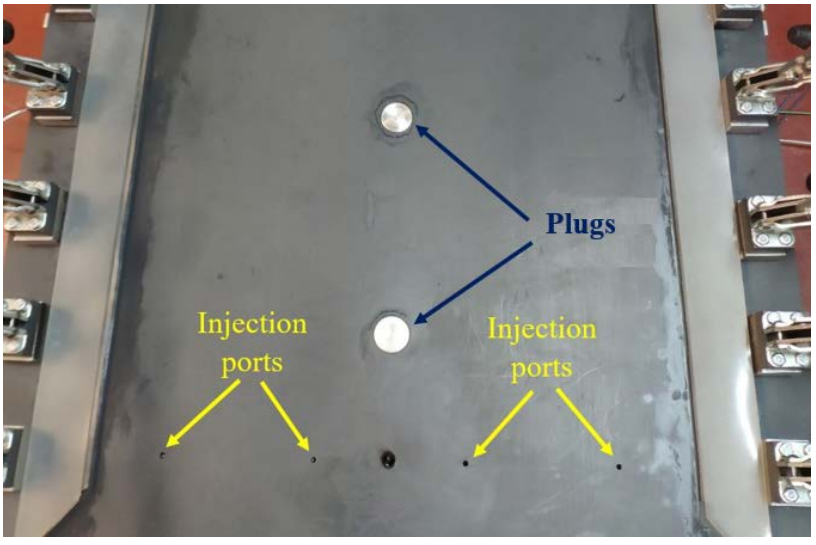

Figure 4.7: Injection ports and plugs.

The fuel, in this case methane, is taken from a bottle as the one shown in Figure 4.8a under a pressure of 0.3 bar whereas the air is taken from the environment and passed through a valve, like the one pictured in Figure 4.8b, which increases its pressure up to 5 bar. This value is the minimum one required by the actuators for their right functioning.

To obtain the desired equivalence ratio, each gas is controlled and regulated by a mass flow controller, as presented in Figure 4.8c (Sierra SmartTrack 100 for fuel and Omega FMA5418A for air).

At this point, the air coming from the valve of Figure 4.8b is divided into two different circuits: the one used to feed the actuators at 5 bar, and the one employed to feed the mass flow controller. As this device cannot work with a pressure higher than 2 bar, a pressure regulator as the one of Figure 4.8d is needed to reduce the pressure from 5 to 2 bar.

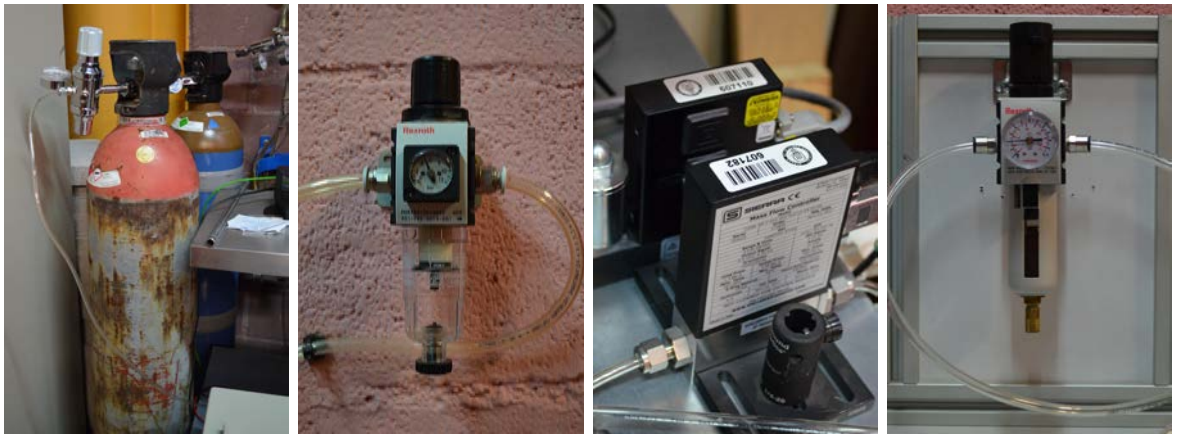

(a) (b) (c) (d)

Figure 4.8: Components used: **(a)** methane bottle, **(b)** high pressure regulator, **(c)** mass flow controllers and **(d)** low pressure regulator.

Air and methane are then mixed before entering into the combustion chamber. This process is carried out in a gas mixer (Figure 4.9) composed by two inlet tubes and one outlet tube, which is connected to a ball valve (used as a security mechanism).

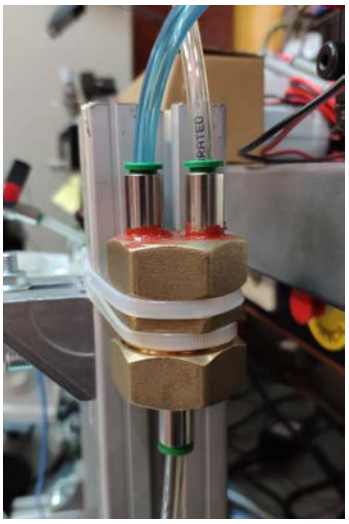

Figure 4.9: Mixer.

All the elements mentioned above (switch, air/fuel mass flow controllers and actuators) have been included in the developed LabVIEW program and hence, can be controlled from the computer thanks to the electronic circuit built in Figure 4.10.

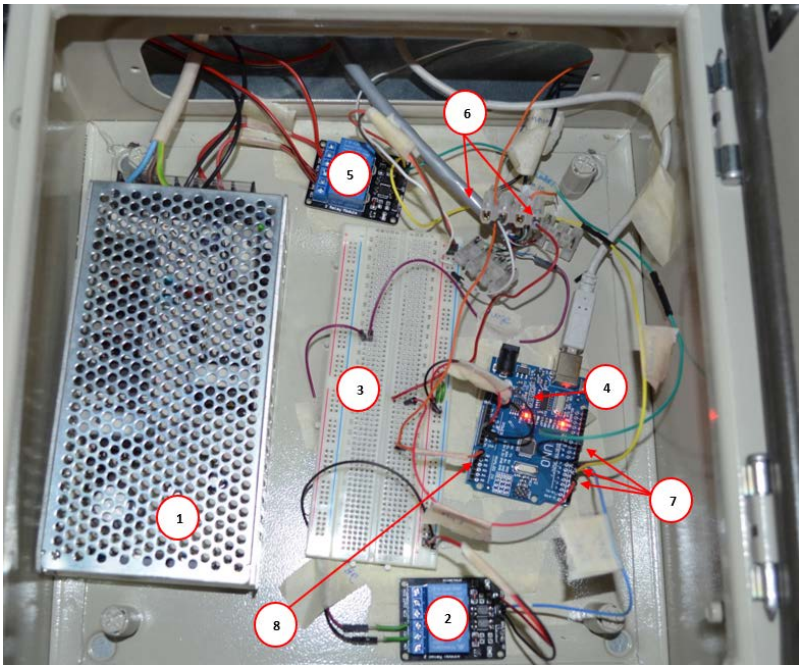

Figure 4.10: Electric circuit stored in a security box.

For that purpose, an Arduino microcontroller (4) together with a protoboard (3) and three relays (2;5) have been employed. As these electrical components can be easily modified, it has been decided to store them (power source of the actuators (1) included) all together in a security box as the one of Figure 4.11 so nobody can touch it nor modify it accidentally.

Figure 4.11: Security box containing the electronics.

The interior of this box is represented in Figure 4.10. Nonetheless, a more detailed schematic containing all the electronics of the experiment can be found in Appendix B.

The function of the relays is basically to open or close the electric circuit so the instrument of interest gets activated or not. In this case, it has been used for the two actuators (5) and for the activation of the air purge (2) to clean the cell after each experiment. In both cases, the circuit is normally open and if the relay receives a small voltage from Arduino, the circuit closes and so the actuators or the purge start working.

Note that although the air purge works with a relay, the normal control of the air flow behaves in a different way (to be explained in Section 5.2.1) and therefore, the manner in which they communicate with the computer is distinct (purge needs a relay whereas the air supplied during the filling does not). In any case, all the electronics coming from the Omega controller are together in the grey big cable (6). For the control of methane no wiring in the security box is needed since the controller device is directly connected to the computer via a COM port.

The rest of the cables linked to the protoboard and Arduino shown in Figure 4.10 make possible the connection and well functioning between the elements described above and the computer. In all the cases, the microcontroller digital ports (7) are used with the exception of the switch, which uses an analog one (8). The explanation of this will be given in more detail in Section 5.2.1.

As a clarification, the main difference between the digital and analog entries is that the former produces an output voltage with only two values, high and low, whereas the latter reads an input voltage which can assume any value within a range.

The last two important items utilized in this experimental setup are the high-speed digital camera "Memrecam HX3", shown in Figure 4.12a, able to take sequences of high-definition images at 2000 fps (frames per second) and the DAQ, a charge amplifier which collects the pressure and acceleration information measured by the sensors described above. The idea with this equipment is to study the noise signal at each instant of time and compare it with the actual frame taken by the camera.

(a) Memrecam HX3.

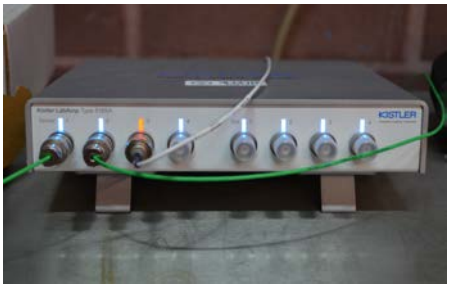

(b) Kistler labamp 5165a

Figure 4.12: Components used: **(a)** high-speed camera and **(b)** DAQ charge amplifier.

In order to make it clearer so the reader has a better understanding of the setup, a summary with most of the parts described in this section can be found in the schematic of Figure 4.13. Here, the system of reference used, the location of the glow plug, the injection ports and the high-speed camera, as well as the way the flame propagates from the left end to the right one are described.

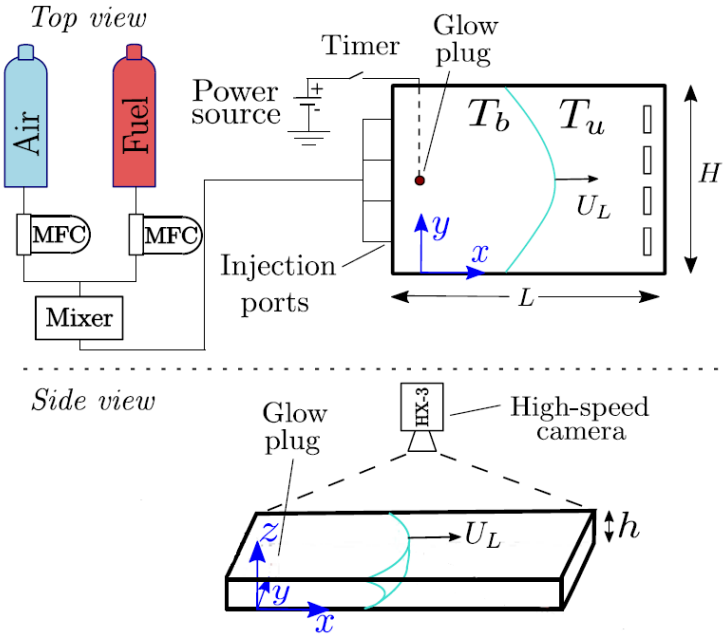

Figure 4.13: Schematic representation of the experimental apparatus [20].

4.2 Main changes with respect to the previous design

All the elements described in Section 4.1 are the ones present today. However, there has been some changes since this project was started that is important to comment.

First of all, a 10 mm-thick PVC sheet has been placed so as to put up the sensors (which were not there before). For that purpose, the aluminum table has been drilled, causing a great impact to the performance of the experiment as it will be explained later.

In turn, the structure has been reinforced by adding three more legs in the middle of the cell and by putting bolts in order to join better all the parts. Moreover, the use of actuators has forced the implementation of an extra structure.

In Figure 4.14 reader can see the configuration of the Hele-Shaw cell before all these modifications.

Figure 4.14: Hele-Shaw cell appearance before changes [34].

The sum of all these factors has provoked some differences with respect to what F. Veiga et al show in [20] as these structural changes affect the interaction of the cell with the flame, and more specifically, the development of acoustic instabilities (see Section 6.4).

4.3 Procedure

After describing the function of every single gadget taking part in the experiment, in this section the procedure followed in each ignition will be explained (for further information, consult the user's guide in Appendix A). This process can be divided into four stages: set up, filling, combustion and cleaning.

Set up:

The first step is always to prepare all the electronic components for its right functioning, that is, to plug in and switch on the DAQ, the camera, the battery, the actuators power source, the mass flow controllers and of course, the computer. In this step, the user must also connect the Arduino microcontroller to the computer via USB, and the camera, DAQ and fuel controller through a COM port.

In this preliminary stage, before the experiment is initiated, the camera must be placed on a tripod at the right spot above the cell so it can record the whole trajectory of the flame. It must be calibrated with its own software so it has the right balance of colours, the appropriate focus and it is verified that its position is the most adequate one. The pressure and accelerometer sensors are usually in place, but in the case this does not happen, it will be necessary to install and connect them as well.

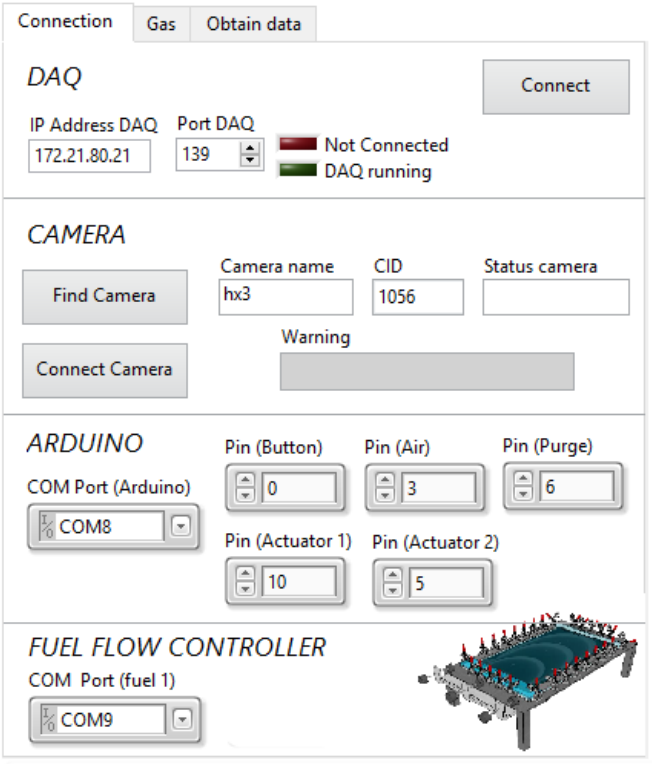

Figure 4.15: LabVIEW screenshot of the connection tab.

Finally, the gas valves must be opened. As explained in the previous section, methane has to leave the bottle at a working pressure of 0.3 bar whereas the air valve must be set to 5 bar (taking into account that the second valve of Figure 4.8d is always maintained at 2 bar). When everything is ready and safe, the different security valves distributed along the circuit must be open so the gases can flow.

At this point, the LabVIEW computer program comes into play since it will be the point from which the user will be able to control all the possible devices employed in the experiment. For that purpose, the user will have to connect the camera, DAQ, Arduino and fuel controller selecting the correct port number or IP address (maintained constant in all the tests) so the program is able to recognize and communicate with them, as illustrated in Figure 4.15.

Filling:

To start the filling, the Hele-Shaw cell is set to closed-open configuration, that is, "actuator 1" seals the ignition end while the opposite end of the vessel remains open for venting during the filling. Although this is the current configuration used in the lab, the program allows to choose among all the possible boundary conditions in case it is wanted to study other conditions (open-open, open-closed, closed-closed, closed-open).

The user then configures the mass flow values so the desired equivalence ratio is achieved. For that purpose, the flow of air remains constant at 2.4 SLPM (Standard Litre Per Minute) whereas the methane flow rate is changed following the Table 4.

Table 4: Equivalence ratio as a function of the methane mass flow rate.

ϕ	0.7	**0.8**	0.9	**1.0**	1.1	**1.2**	1.3	1.4
Mass flow rate [g/min]	0.117	**0.134**	0.151	**0.166**	0.185	**0.201**	0.218	0.235

Once ϕ is fixed, both the air and fuel valves can be open from LabVIEW setting the filling time to two or three minutes. This is the estimated time it is required for the gases to distribute inside the cell taking into account the mass flow rate of the mixture, the volume of the combustion chamber and the density of the mixture ($t = Volume \cdot \rho/\dot{m}$).

Upon the complete charge, the program closes automatically the supply of air and methane. The user then has to order the activation of "Actuator 2", keeping both ends shut to allow the gases to come to rest. Immediately after, the ignition injection end is reopened (open-closed configuration) and the mixture is ignited by pressing the green button which connects the battery and the glow plug (the amount of electrical energy supplied is held constant for all the experiments).

Combustion:

The same green button ignites the flame and activates the camera and DAQ with a delay that can be set previously if it is known that the time it takes to burn the mixture is longer than usual (the memory of the camera is limited and thus, the recording time).

During this brief instant of time (1-2 seconds), the luminous emission of the flame will be registered by the high-speed camera catching every single detail of the propagation of the wave (shooting at 1000 fps). Similarly, the DAQ will plot the corresponding signal with the information captured by the pressure and acceleration sensors. This data will be stored in a text file with a predefined route established by the user.

Cell cleaning:

Right after the flame is consumed, it is advisable to clean the cell with fresh air so no fuel nor combustion products (e.g. condensed water) remains there for future experiments, modifying and disturbing in this way future results. As in the filling process, the vessel needs to be in closed-open configuration so the gas goes from one end to the other. However, in this case only air is going to be employed. To this effect, purge will be activated during at least one minute after which it will stop automatically.

As a final remark and for security reasons, it is recommended to leave both actuators deactivated leaving the cell in open-open configuration and ready for the next test.

5 Automatization of the process with LabVIEW

The main objective before starting this project was to develop a program so the signal recorded by the pressure sensors was synchronized with the images provided by the slow motion camera. In this way, the user would be able to carry out an accurate and deep study of the propagation of premixed flames. This necessity arose due to the fact that each device had its own software. As a consequence, it was not possible to start the functioning of both instruments without provoking a small, unknown and immeasurable time difference between them, therefore leading to a wrong and more complicated analysis as there was no chance of relating each frame with a pair of pressure data.

Once achieved this main goal, in order to make the procedure easier, finer and improved, it was decided to implement one by one the rest of the components in the code (air and fuel mass flow controllers, switch and actuators). Now, thanks to this program every variable can be controlled from the same point, thus avoiding losing time and having different codes, and at the same time providing the experiment with more accuracy and repeatability.

5.1 About LabVIEW

Before starting explaining in a detailed way the procedure followed in LabVIEW, it is advisable to give a short overview of the program in case the reader is not familiarized with it.

Programming in LabVIEW is somehow different to the rest of the programming languages since here the code itself is graphical (the programming language is officially named "G"). There is no text based code, but it is a diagrammatic view of how the data flows through the program. Moreover, there are two windows instead of just one; the programmer has to deal with two different interfaces: the front panel and the block diagram.

The former, the front panel, is the user-friendly side of the program. It is basically the window the user interacts with and the face of the software itself. Most of the figures presented later on in this report represent this side. The other one, the block diagram, is where the real code is created and where the programmer works. This language is denoted as visual because the program is built upon joining different items (blocks) in order to develop whatever is wanted. An example of this can be found in Figure 5.1. Here, a small part of the final code is presented, more specifically, a while loop containing the necessary items for the actuators, the green button, the air and fuel filling and the air purge.

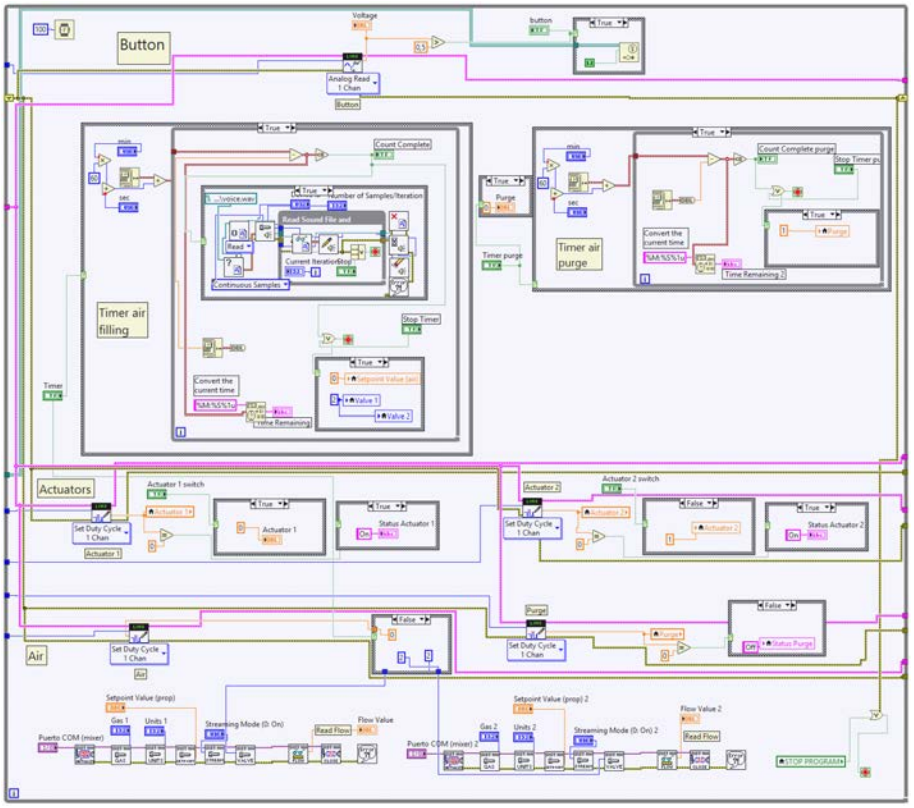

Figure 5.1: Example of the block diagram interface.

5.2 The design process

As a starting point, both the camera and DAQ drivers developed for LabVIEW by the manufacturers were used. These programs were too complex and had a lot of features that were not useful for this particular case, which made them being slow and inefficient. Thereby, a first step was to "clean" and remove every detail that was not of help on the condition that the correct functioning was guaranteed.

Figure 5.2 shows the main aspects (in red) that have been taken away from the initial camera LabVIEW code. Most of them are related to the configuration of the device such as the frame rate at which it has to record or the colour balance, as from the beginning it was decided that all these parameters were going to be tuned through the actual program of the camera (i.e., not in LabVIEW). In yellow it can be seen one of the many words bugged (specially in the block diagram) that had to be fixed in order to understand it better. Finally, in green (Event and debug data), all the factors that are essential for the right functioning of the software but do not need to be changed by the user. For that reason, it was decided to hide them so they do not disturb and occupy space in the screen.

In addition to that, the video screen was resized due to the fact that it had a large

zoom and made it difficult to watch the whole field of view offered by the camera (the user had to scroll up and down, left and right).

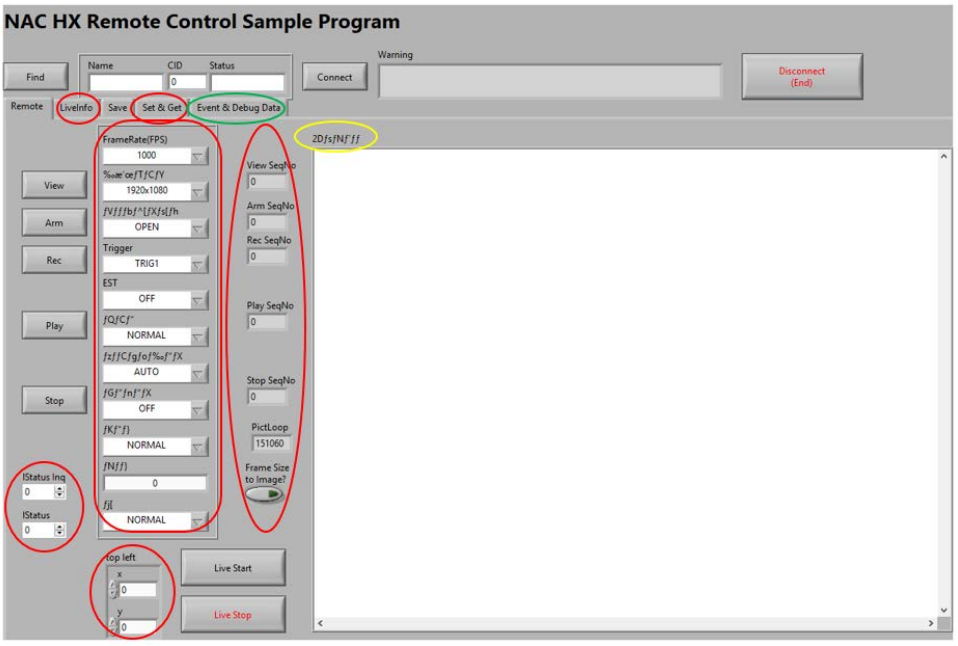

Figure 5.2: Original camera software provided by NAC.

Similarly, Figure 5.3 represents the main changes carried out for the DAQ case. Following the same legend as before, red colour means deleted item whereas green colour means necessary item but hidden.

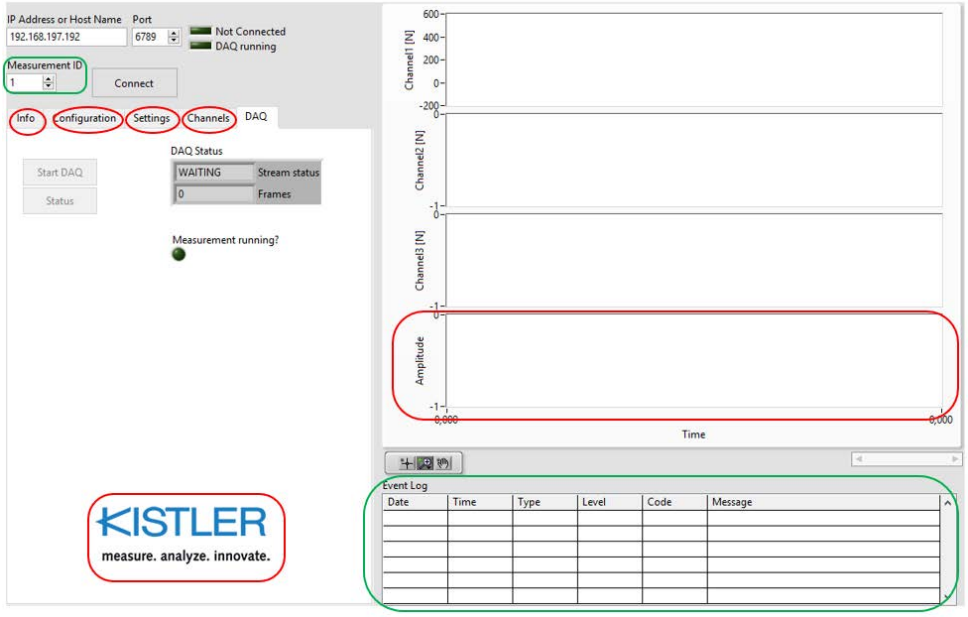

Figure 5.3: DAQ software.

It has to be remarked that at this point there was a number of characteristics that were withdrawn with no apparent effect and it was not until later stages of the process that it was noticeable and crucial to come back as the program did not react properly to some responses.

The next step and one of the most important of the process was to merge both programs into a single one. Here a lot of difficulties were found since the way the codes were written was completely different, so it was needed to choose only one of them (DAQ), and rewrite and adapt the other one (camera) so the two front panels and block diagrams were just one.

Over the course of this particular step, even if it does not seem like an important issue, the main trouble has been to find the way to stop the program. Since both drivers had different ways of exiting, the idea was to have just one that worked for both of them. However, it has been impossible.

The way the DAQ worked was by directly closing the principal tab whereas the form the camera quit was by pressing a button (shown at the top-right of Figure 5.2 as 'disconnect-end'). Finally, the solution achieved was to maintain both methods but leaving the DAQ manner as the main mechanism to exit since it works for all the components.

To clarify, the program can only be disconnected with the mentioned button ('disconnect-end') if the DAQ is not connected. If the DAQ is present, the only possibility is to close the principal tab. Despite what the reader may think, this redundancy cannot be avoided since both structures are needed for the right functioning of the software.

At this point, the appearance of the program was similar to the one displayed in Figure 5.4.

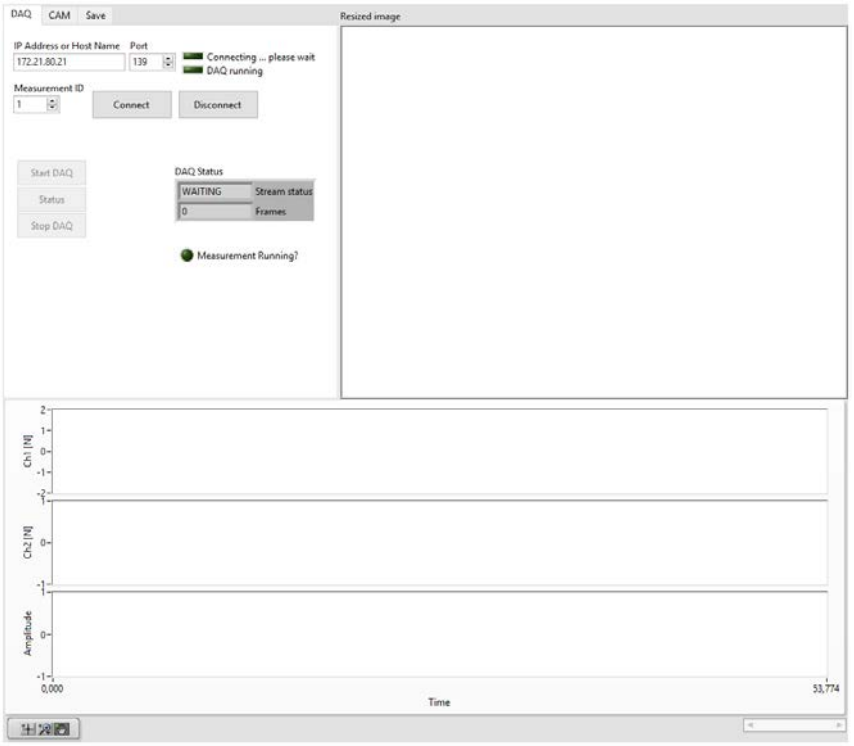

Figure 5.4: First approach of the merged program.

Here, the starting of the data recording (video and pressure) was still split, so the time gap between them was present anyway. In order to fix that, the 'START DAQ' (of Figure 5.4) and the 'REC' (of Figure 5.2) buttons were unified in such a way that by clicking on the same knob, both devices started to work (see 'Start DAQ and Cam' button of Figure 5.5, changes in green).

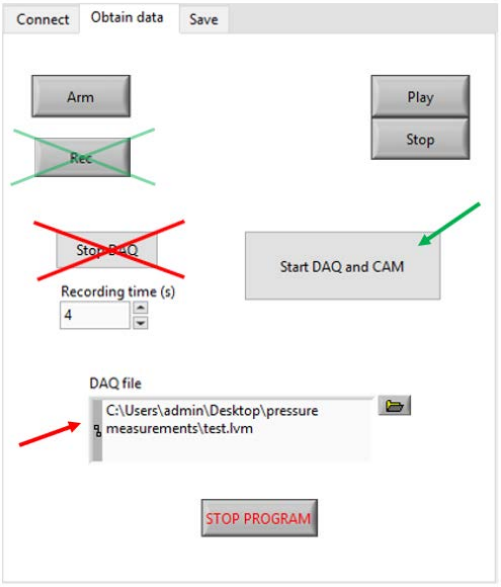

Figure 5.5: Evolution of the merged program

Since the reading of pressure data was configured to be stopped manually, it was decided to create a numeric control so that the user could be able to choose beforehand the amount of time he or she wanted to record (usually around 4 seconds, depending on the mixture). Moreover, a file path control was enabled to store these pressure data in the desired folder with the wished name (see Figure 5.5, changes in red).

5.2.1 Further steps

At this stage, taking into account that the camera and DAQ were finally synchronized, the aim of the project was already fulfilled. Nonetheless, it was not the most sophisticated it could be since the filling of the fuel and air was executed from another program, the ignition of the flame was carried out with the green button but it was not synchronized with LabVIEW (i.e., the user had to click at the same time the 'Start DAQ and CAM' control and the green switch), the actuators were not present and hence, the user had to open and close the combustion chamber manually (thus losing accuracy due to the leak of a small portion of the gas) and in general, the experiment was not so automated as to accomplish it without at least two people.

Therefore, the next step beyond the main objective of the project, was to improve all those points.

The first one was related to the switch. The way this has been implemented in the code has been through Arduino. When the green button is pressed (physically), a small voltage difference is sent to this microcontroller. The signal is then read by an analog pin, which transforms the electric impulse into a numeric value. This value is transmitted to the computer via USB and to LabVIEW using the code shown in Figure 5.6.

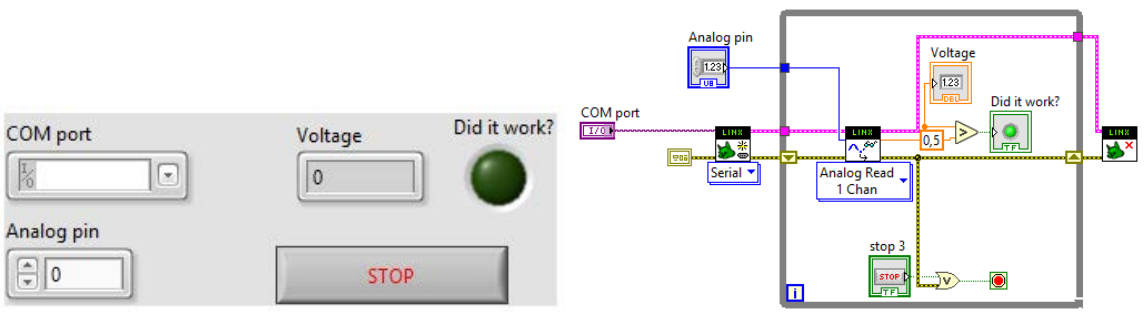

(a) (b)

Figure 5.6: LabVIEW code used for the switch: **(a)** front panel and **(b)** block diagram.

Once it was possible to obtain a signal in the computer every time the switch was activated, it was needed to implement it in the main code. This task was difficult at the beginning because it implied that the 'true' value coming from the boolean (shown in Figure 5.6a) activated internally the 'Start DAQ and CAM' key (which in the past was turned on by the user). Considering how LabVIEW works, this could not be done intuitively. After trying several methods, finally it was discovered that it was necessary to create what is known as a 'user event' in order to programmatically trigger such an event ("User events allow different parts of an application to communicate asynchronously. Unlike user interface events, which require direct user interaction with front panel objects, user events allow the creation of an application that responds to programmatic changes on objects" [37]).

As the recording time capacity of the camera is limited (up to four seconds approximately), sometimes depending on the mixture to be burnt, this amount of time is not enough to catch the whole propagation. For those flames unable to start the ignition within the limits, it was decided to install a delay so the user is able to manage the time between the switching-on of the glow plug and the starting of the recording.

The next level was to control the gases with LabVIEW too. Previously, the air was always set to constant and the fuel was tuned through the software "Smart Track 2". As they worked differently, the way they have been included in the code has been distinct as well.

Regarding the air, whose mass flow controller is the Omega FMA5418A, the connection has been done through electronics (see Section 4.1 and Appendix B). Following the instructions of the manufacturer, the flow of air when filling the chamber needs to be set providing a voltage between 0 and 5 V_{DC}. To that end, the device has been connected to a digital pin of Arduino so the right voltage can be supplied from the program. In this case, the value of 0.475 has been selected in order to have an airflow of 2.4 g/min.

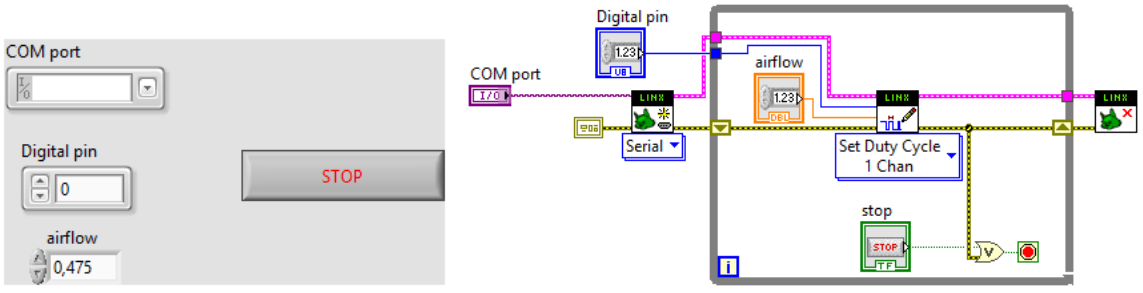

(a) (b)

Figure 5.7: LabVIEW code used for the air flow control: **(a)** front panel and **(b)** block diagram.

Following a similar procedure as with the switch, the software for the air control is shown in Figure 5.7. Notice that this fragment of code is simple and short because it is the minimum required to work alone without any other device. Hence, when being incorporated into the main program, difficulties arise.

The principal obstacle has to do with how to start and to stop the air flow. In order to solve this and to make the filling process easier, a timer has been developed (see Figure 5.8).

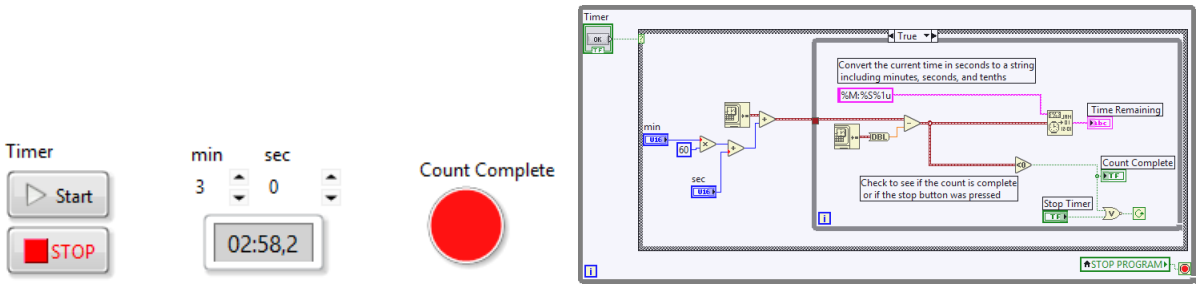

(a) (b)

Figure 5.8: LabVIEW code used for the countdown: **(a)** front panel and **(b)** block diagram.

With this gadget, apart from having the countdown incorporated (usually 3 minutes), the air filling starts as soon as the user clicks the start button and stops either if the user decides to stop the chronometer or if the time is over. The way this has been achieved is by simply giving the value of 0.475 V_{DC} (or any other value provided by the user in case it is not wanted to have the 2.4 SLPM) if the start key is hit, and 0 otherwise (marked with a red arrow in Figure 5.10b).

Directly related with the air, but not with the filling, is the purge. As commented in Section 4.3, once the combustion is finished, the air purge is activated during 1 minute, approximately, in order to clean the cell and remove any unburnt remainder of fuel. Its activation in LabVIEW is pretty similar to the previous case (with a timer) but the electronic part is not.

In this case, again following the instructions of the manufacturer, purge is achieved by joining a specific wire coming from the controller to the common ground. Thereby, unlike the aforementioned event, only two values are possible, on and off. For that purpose, the use of a relay is needed (explained in Section 4.1). This relay connected to a digital pin of Arduino closes or opens the circuit depending on whether it receives a small amount of voltage from it or not. This voltage, as before, is controlled by the LabVIEW software.

In regard to the fuel control, the electronics are much easier as the Sierra SmartTrack mass flow controller can be directly plugged into the computer via COM port. However, the LabVIEW code has been more complicated even though the manufacturer's driver has been used (see Figure 5.9).

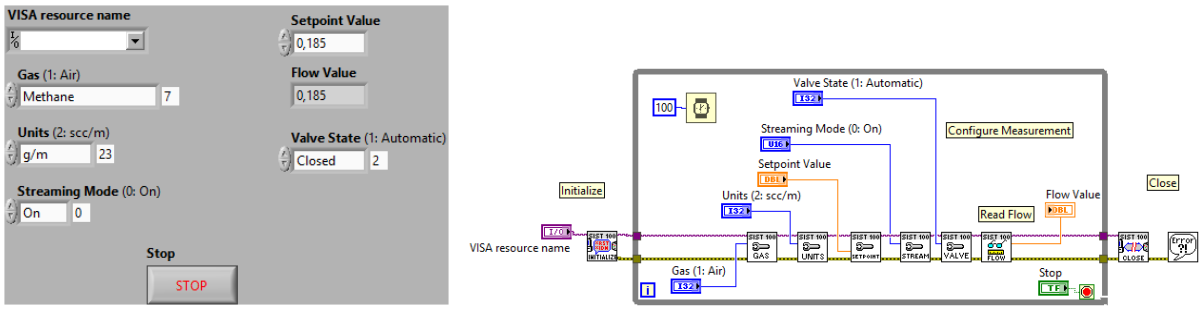

(a) (b)

Figure 5.9: LabVIEW code used for the control of the fuel flow: **(a)** front panel and **(b)** block diagram.

The mode it has been followed for its implementation has been the next one: the user establishes the gas, the units, the setpoint value and opens the valve. However, it is not until he or she presses the start button of the countdown when it actually starts the filling (together with air). As before, if the time is stopped or if it is over, the valve returns to the closed state (giving a value of 2, as shown in Figure 5.10b with the green arrow). This can be done thanks to local variables distributed all around the code (variables that allow data to be passed between parallel loops within the same program).

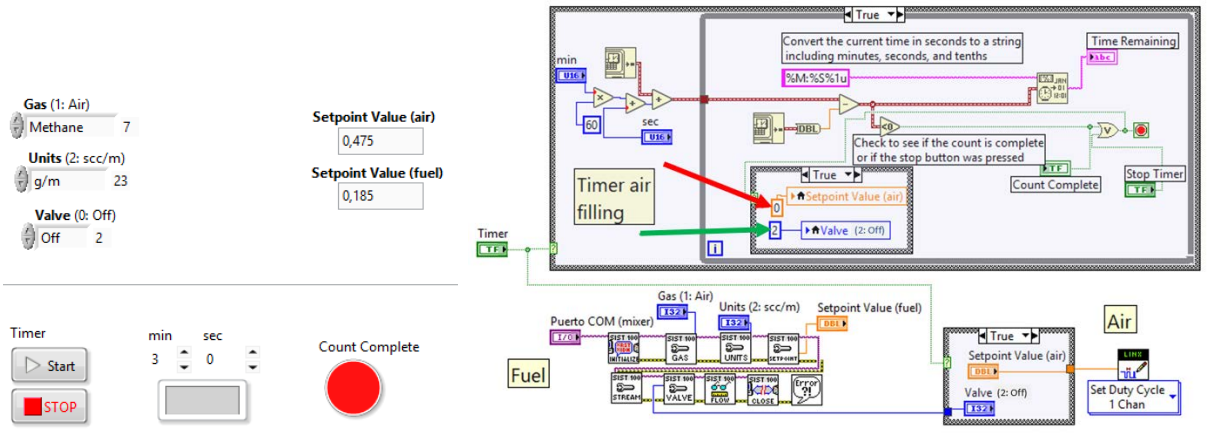

(a) (b)

Figure 5.10: LabVIEW code used for the control of the gases flow: **(a)** front panel and **(b)** block diagram.

Finally, the last ingredient to finish the program has to do with the actuators. As commented in previous sections, at the beginning of the project the opening and closing of the combustion chamber was done manually. In the last months (around April), it was decided to buy two pneumatic actuators to carry out this task.

Its inclusion in LabVIEW has been relatively easy as they work in the same manner as the air purge. These devices have incorporated an electrovalve in each unit so if it receives the needed voltage (provided by the power supply) the actuators close the combustion chamber. That is, if the circuit is opened so it will be the combustion chamber, and if the circuit becomes closed, the actuators will activate. This can be simply controlled with the help of a relay connected to a digital pin of Arduino. The LabVIEW code is exactly the same as the air purge and the electronics can be found in Figure 4.10 or in Appendix B in a schematic way.

For security reasons, the actuators cannot move automatically (for example, when the gas filling is accomplished), so the user has to give the command. Also, once the experiment is done, the actuators should remain deactivated, leaving the combustion chamber completely open. If for any reason the user forgets to do it and closes the program, they will be automatically (only in this case) deactivated.

The last detail that provides the code with a more professional aspect, is the voice message that sounds once the filling has been completed. In case the user is doing another activity during those three minutes and not paying attention to the time, he or she can realize and come back immediately to ignite the flame. Also, it indicates the procedure to follow with the actuators sequence just for helping the user (for the open-closed case). Such code can be consulted in Figure 5.11.

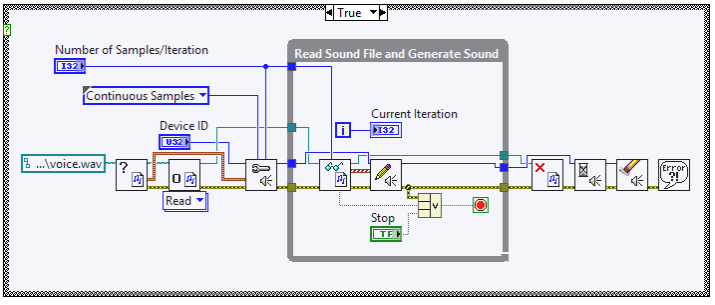

Figure 5.11: LabVIEW code used for the voice message.

As a final remark, it has to be commented that the code cannot be used to save the video. As its size is about 16 GB and cannot be manipulated in LabVIEW (trim and edit), the storage process can take up to more than 20 minutes per experiment. Thereby, as the images remain stored in the camera memory until a new ignition takes place, the user can close the LabVIEW program and open the NAC driver, thus selecting the frames of interest and saving the video in a quicker way.

5.3 Final program

With all the parts being explained, the final program is ready for its use (see Figure 5.12). As the final user does not have to modify anything (in principle), it has been decided to create an '.exe' file so in its daily use the access to the block diagram interface is restricted. Due to the dimensions of the code, the block diagram can be found in Appendix C.

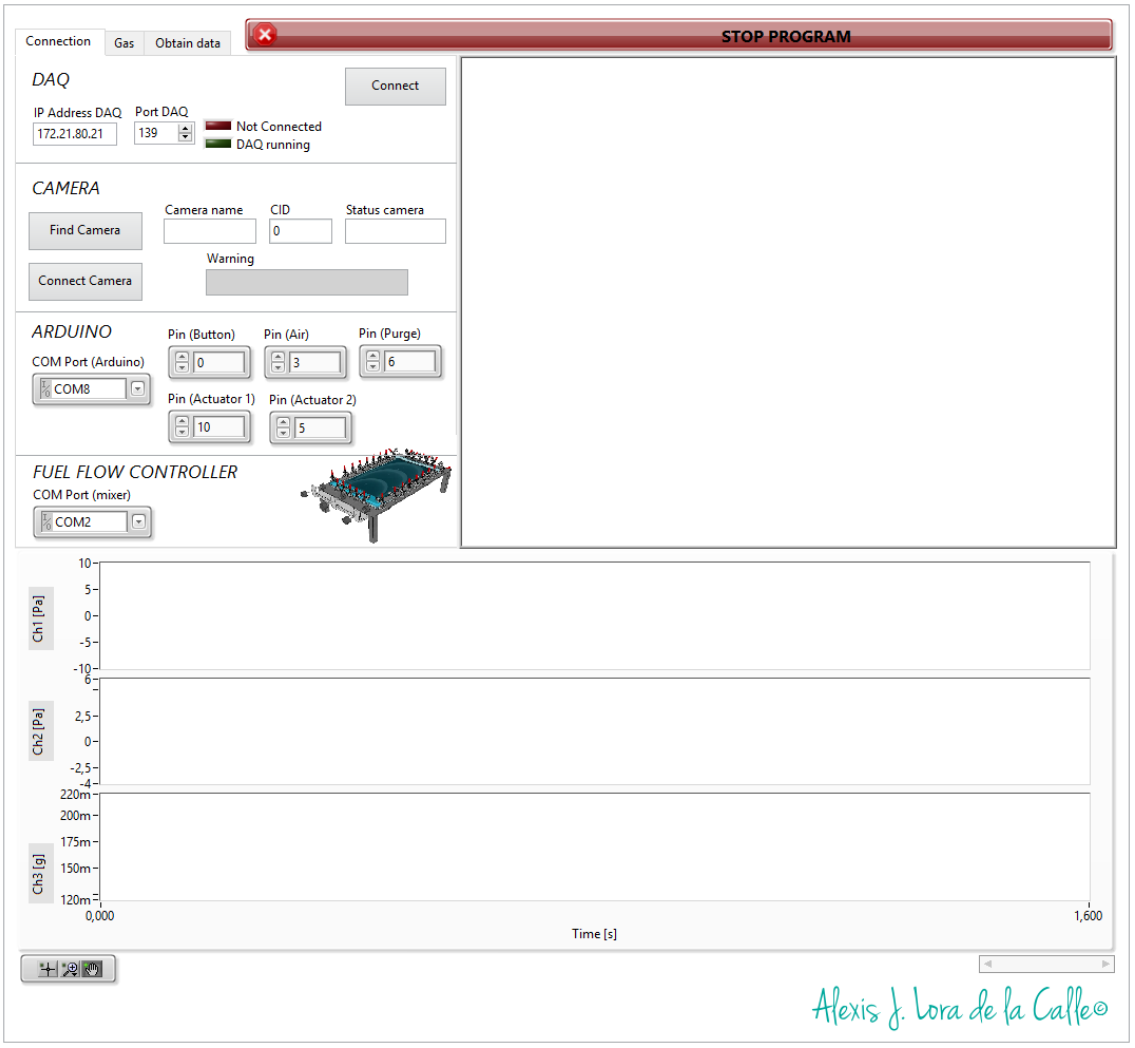

Figure 5.12: LabVIEW final program: front panel.

In Figures 5.13 and 5.14 reader can observe in a detailed way how the front panel looks like while the experiment is being carried out.

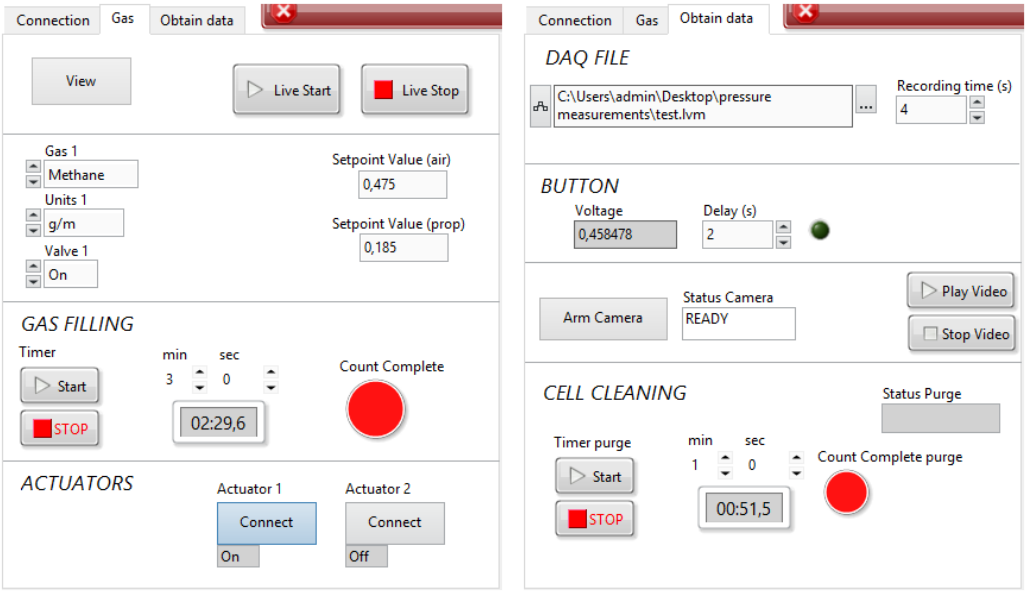

(a) (b)

Figure 5.13: LabVIEW final program: **(a)** gas tab and **(b)** obtain data tab.

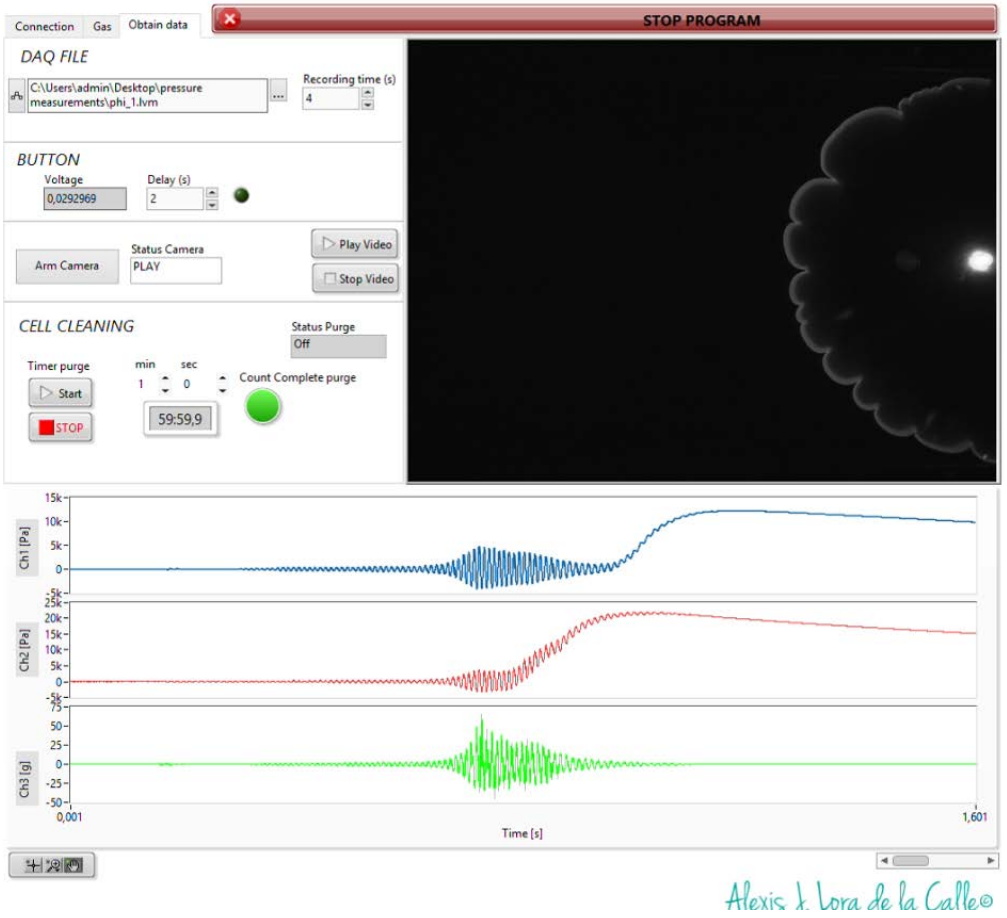

Figure 5.14: LabVIEW final program during experiment.

6 Experimental data analysis

After running an experiment and finishing the ignition, as explained in previous section, two output files are obtained: a text file with extension .lvm containing the pressure and acceleration data recorded by the sensors, and a video file in .mp4 comprising the propagation of the flame through the Hele-Shaw cell.

Therefore, this section will aim at explaining how and with which software these files can be analyzed, and which information can be retrieved from them.

Finally, three cases will be studied using methane as a fuel with the objective of verifying and validating the code: a lean flame (Section 6.2), a stoichiometric flame (Section 6.3) and a rich flame (Section 6.4). It is important to remark that the configuration, procedure and conditions under which the experiment has been carried out have been maintained for all the three cases.

6.1 Image processing

Image processing is the name given to the process through which the different pictures or frames composing the video are digitized or divided into pixels with the objective of improving their quality and making easier the data acquisition.

This procedure is going to be done mainly in MatLab, making use of the codes prepared by Fernando Veiga López, supervisor of this project (see Appendixes D and E).

The first code called "Video processor" presented in Appendix D basically consists in removing the noise from the images and binarizing them into two possible values: 1 if it catches the wave front (white area) and 0 otherwise (black area). In this way, an internal and external contour is created in each frame which serves as an input for the next code. This process can be observed in Figure 6.1.

Sequentially, the script presented in Appendix E called "Analysis of the flame front" must be run. This program calculates the burnt area and the fraction of burnt area over the total area. Moreover, it calculates the instant velocity of the wave by taking the derivative of the area with respect to time. Finally, with this information several plots as the ones presented in the studied cases can be developed.

It is important to notice that sometimes the flame is so violent that the wave front breaks and the area cannot be easily calculated or the contrast is so low that the image cannot be binarized properly. In those cases, a pre-processing can be carried out in the free software called Fiji, with which contrast and gaps (by dilating the white zones) can be quickly solved.

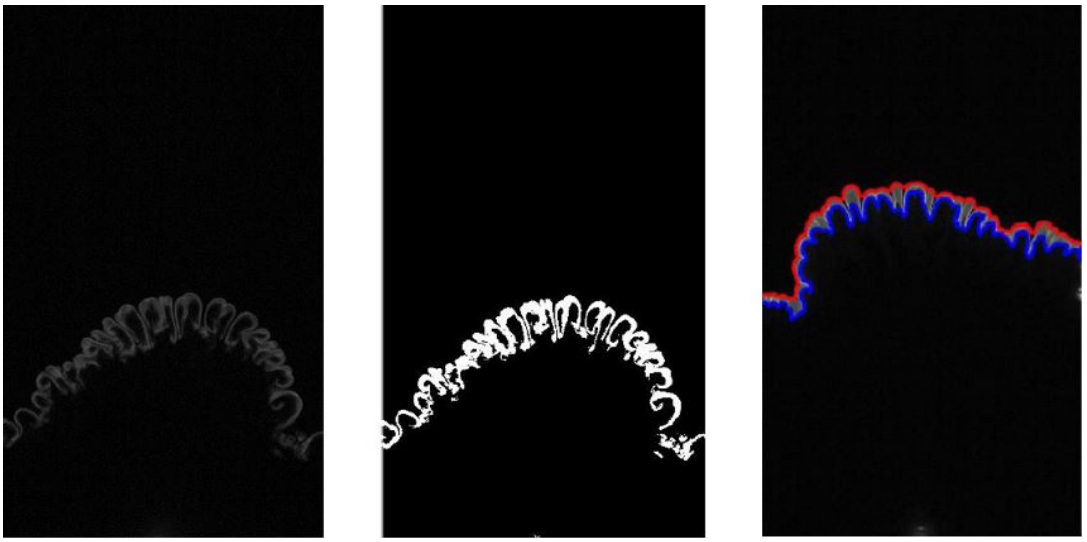

Figure 6.1: Image processing: binarization of the image (center) and obtention of contours (right) [35].

Regarding the processing of the pressure and acceleration signals, it is as simple as importing the .lvm file to MatLab and plot them taking of course into account the time between the first and last frame studied for the computation of the areas and velocities.

6.2 Case 1: lean flame ($\phi = 0.8$)

For this first case, following the Table 4 presented in Section 4.3, an equivalent ratio of 0.8 has been chosen (which corresponds to a lean flame). According to the theory explained in previous sections, the flame front should not be planar, but instead should develop some curvatures as it goes from the glow plug side of the cell to the opposite end.

The first kind of instability that should be observed is the one inherent to all the flames, which is the Darrieus-Landau's. As a consequence, the lean flame should wrinkle to form medium-size cells. As discussed, Diffusive-thermal instabilities should not appear for the case of methane as its Lewis number is approximately the unit ($Le \approx 1$). On the contrary, thermo-acoustic instabilities should play a role as the wave front is being propagated in a confined space.

Notice that as none of the cited perturbations are linked to the equivalence ratio, the differences between the three cases (in terms of instabilities) should not be disparate.

If the reader observes Figure 6.2 will realize that in fact these 2 phenomena take place. In order to understand better this picture, four phases could be distinguished.

The flame starts first right at the ignition point presenting a semicircular shape with a smooth front (not represented in the figure due to the superposition with the next stage). Soon after, it wrinkles to form medium-size cells due to the density variation across the front (DL). From this point, the wave front moves slowly as it undergoes an oscillation of small amplitude, characteristic of the first thermo-acoustic instability. This ends up provoking its flattening at the neighboring of the first quarter of the chamber. Right after, when the reactive front progresses towards the half of the chamber, it can be perceived that the oscillations grow rapidly in amplitude and frequency, thus accelerating the flame (second thermo-acoustic instability). This makes the flame adopt a marked cellular finger-like shape that lasts until it reaches the end of the chamber.

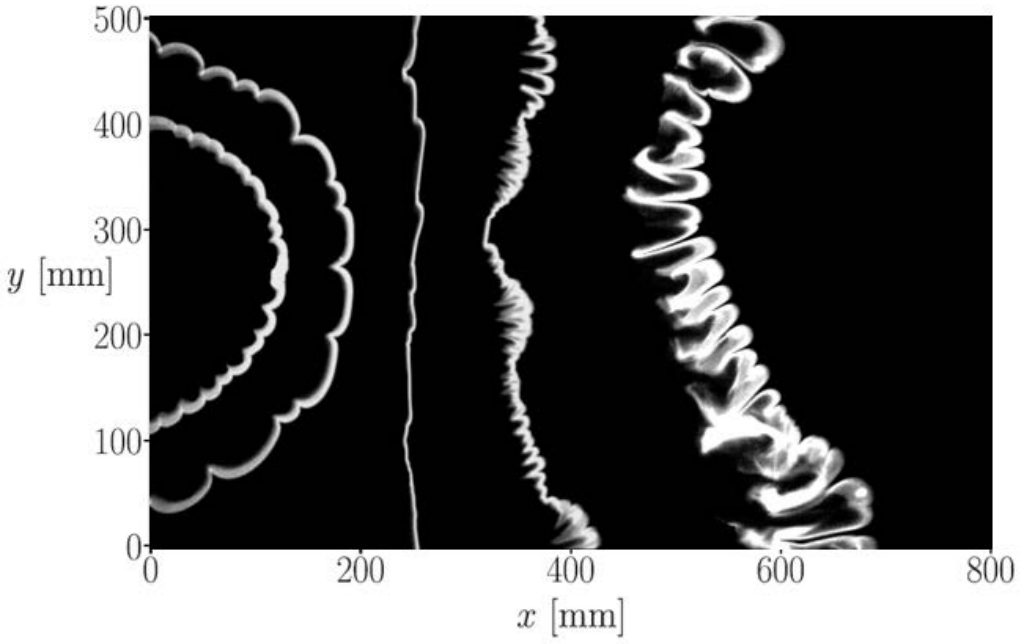

Figure 6.2: Flame front evolution propagating at $\phi = 0.8$.

This oscillatory phenomenon is provoked simultaneously by two factors. On the one hand, the thermo-acoustic instability produced due to the coupling of the acoustic wave with the advancing flame front. This coupling modifies its velocity as a consequence of local pressure variations and hence, it accelerates the burnt mixture producing wrinkling. On the other hand, the confinement of the fresh mixture gases between the flame and the closed end of the cell causes a force on the front accelerating it in the opposed direction [34].

In Figure 6.3 reader can find both the burnt area fraction (left) and the flame velocity (right) as a function of time for this lean case.

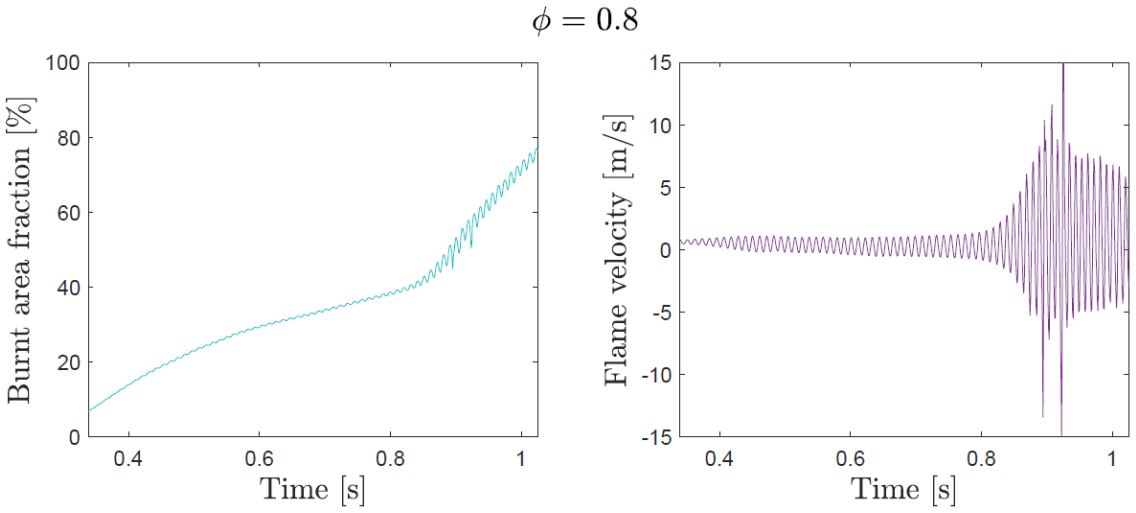

Figure 6.3: Plots obtained after image processing: burnt area fraction in percentage at the left, flame velocity at the right for the lean case ($\phi = 0.8$).

The left plot shows how the tendency at which the burnt area fraction develops is not linear. In fact, it can be observed again this oscillation as the percentage varies up and down. This can be ratified with the plot of the right, where positive and negative velocities reflect that the flame actually moves back and forth while it advances.

Also, it can be seen how slow the flame is at the beginning (around 1 m/s) and how strong and abrupt it becomes as it approaches the half of the chamber (approximately at $t = 0.85$ s and $Area_b = 45\%$), moment at which the speed increases and thus, finger-like shape cells appear as a consequence of the thermo-acoustic instability. From this point on, the velocity increases (peaking at 15 m/s) and hence the rate at which it burns the fresh mixture also rises, leading to a deeper slope, as it can be noticed in the left plot.

Finally, in Figure 6.4 the data recorded by the sensors and accelerometer can be found. Notice that the two plots on the top represent the acoustic pressure of sensors 1 and 2, located respectively at the end and 75% of the combustion chamber (see Figure 4.5). These locations are strategically chosen in accordance to what is known as "piston effect", by which the flame behaves like a piston compressing all the fresh fluid in front of it. That is the reason why the sensors are placed at the end of the chamber, so as to measure the pressure for as long as possible.

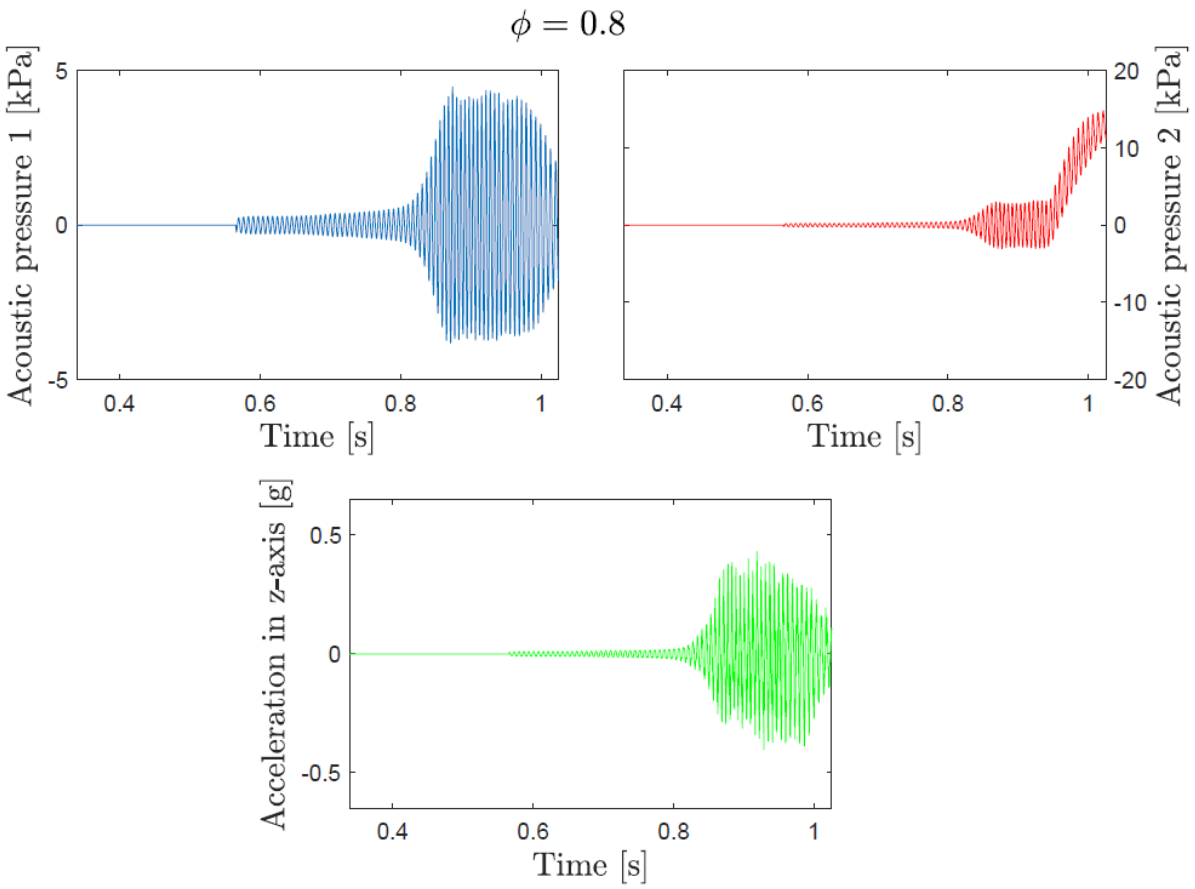

Figure 6.4: Data obtained from the sensors: acoustic pressure of sensor 1 and 2 at the top, respectively, and acceleration of the vertical component at the bottom for the lean case ($\phi = 0.8$).

It can be perceived how the three of them peak at $t = 0.85$ s since it is the moment at which the flame is the most violent. A great difference can be pointed out between the acoustic pressure recorded by sensors 1 and 2, being their magnitudes of 5 kPa and 15 kPa respectively, as a consequence of the difference in behaviour of the flame as it passes through those locations. This is reasonable because the burnt mixture has more energy at the 75% of the chamber than at the end, where the flame can no longer burn more fuel and thus it fades.

6.3 Case 2: stoichiometric flame ($\phi = 1.0$)

For the stoichiometric case, the general trends remain unaltered as it can be extracted from Figure 6.5. The same instabilities and shapes appear and the behaviour is practically similar.

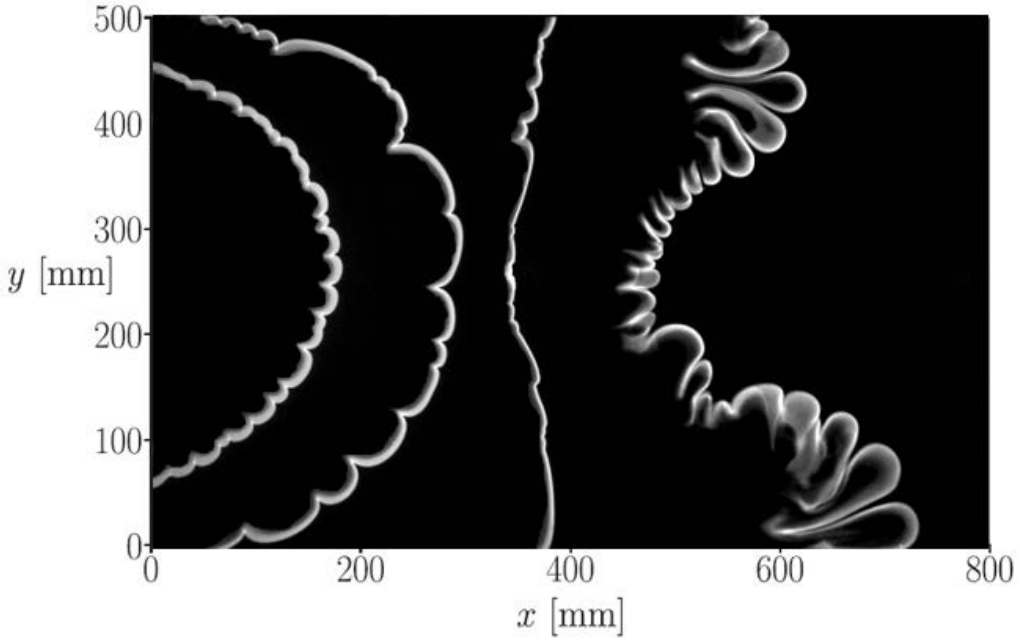

Figure 6.5: Flame front evolution propagating at $\phi = 1.0$.

Contrasting Figures 6.3 and 6.6, one of the main differences with respect to the previous case, although minimum, is the time at which the second instability takes place, being at $t_2 = 0.78$ s as compared to $t_1 = 0.85$ s. Therefore, it can be stated that the stoichiometric flame is a little bit faster than the lean one.

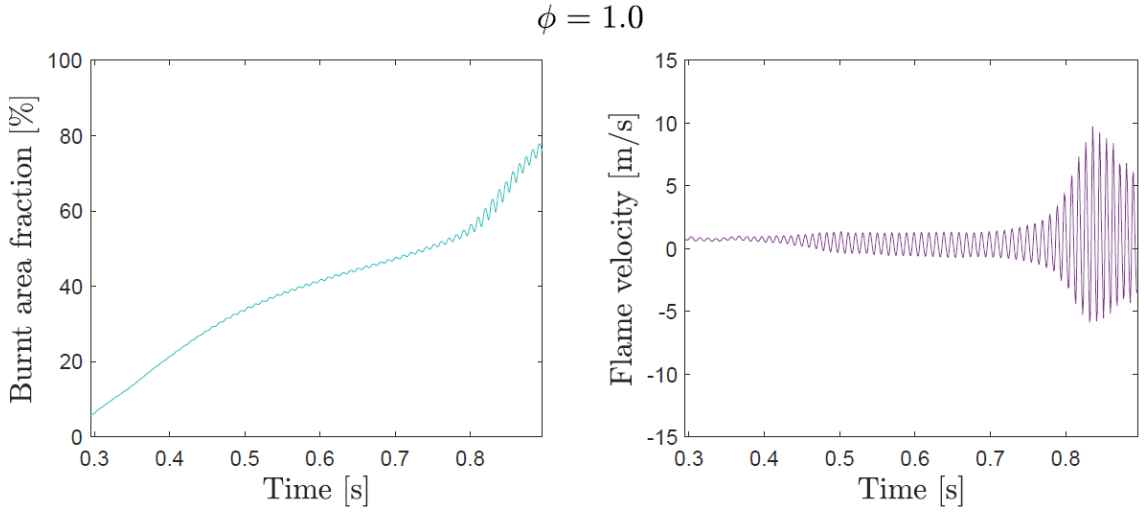

Figure 6.6: Plots obtained after image processing: burnt area fraction in percentage at the left, flame velocity at the right for the lean case ($\phi = 1.0$).

However, this flame of equivalence ratio equals to 1 can be assumed to be less violent if one compares the maximum velocity of this case (10 m/s) against the previous one (15 m/s).

In regards to the signal provided by the sensors and accelerometer, it is clearly visible that the shape and range of values does not suffer substantial changes with respect to the prior sample.

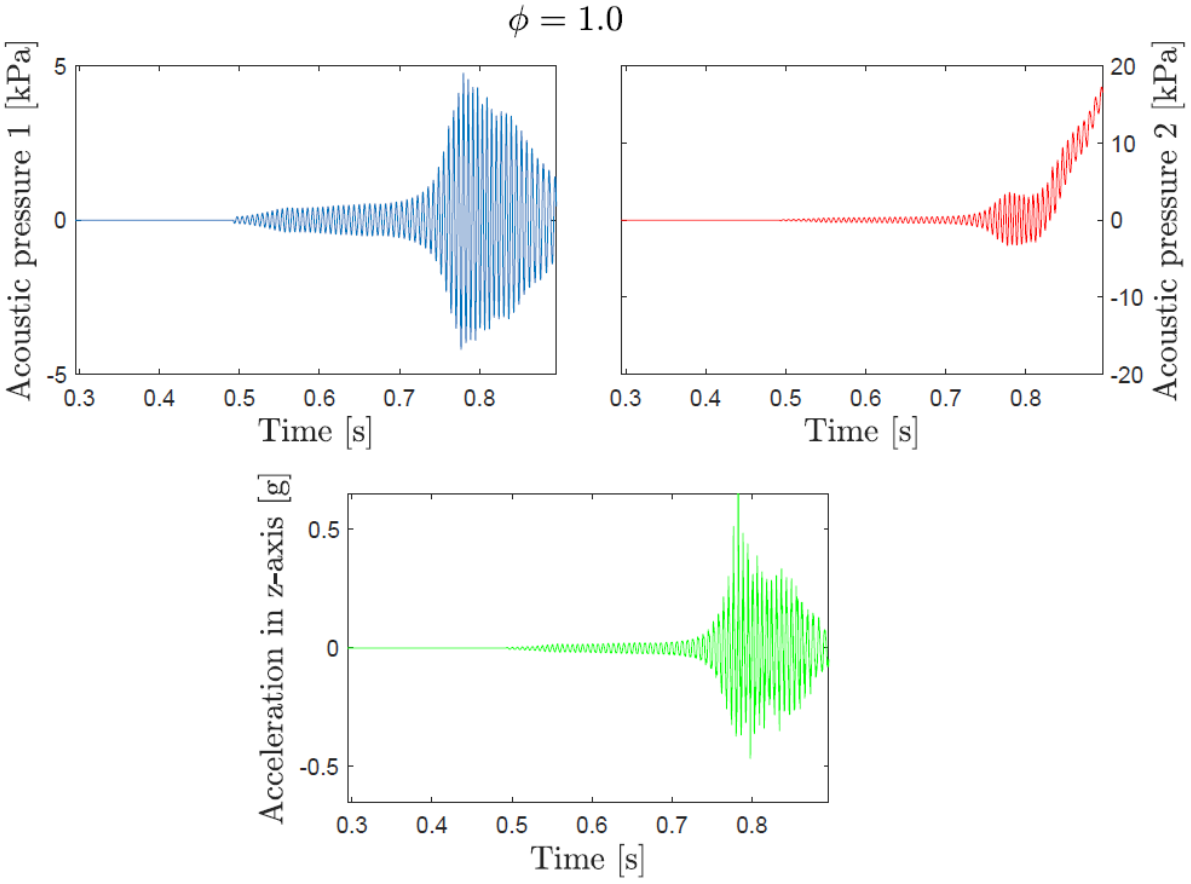

Figure 6.7: Data obtained from the sensors: acoustic pressure of sensor 1 and 2 at the top, respectively, and acceleration of the vertical component at the bottom for the lean case ($\phi = 1.0$).

6.4 Case 3: rich flame ($\phi = 1.2$)

Finally, a rich flame was studied with an equivalence ratio of 1.2. Again, the flame presents the same shapes and perturbations as the equivalence ratio is not directly linked to any of the instability mechanisms.

Nonetheless, in this case it is more clear how the flame develops at the beginning, with that smooth front that did not appear in previous cases due to the superposition of different stages, but it does at the left hand side of Figure 6.8. One of the main reasons why this form come in to view here, is that the rich flame is slower than the former ones.

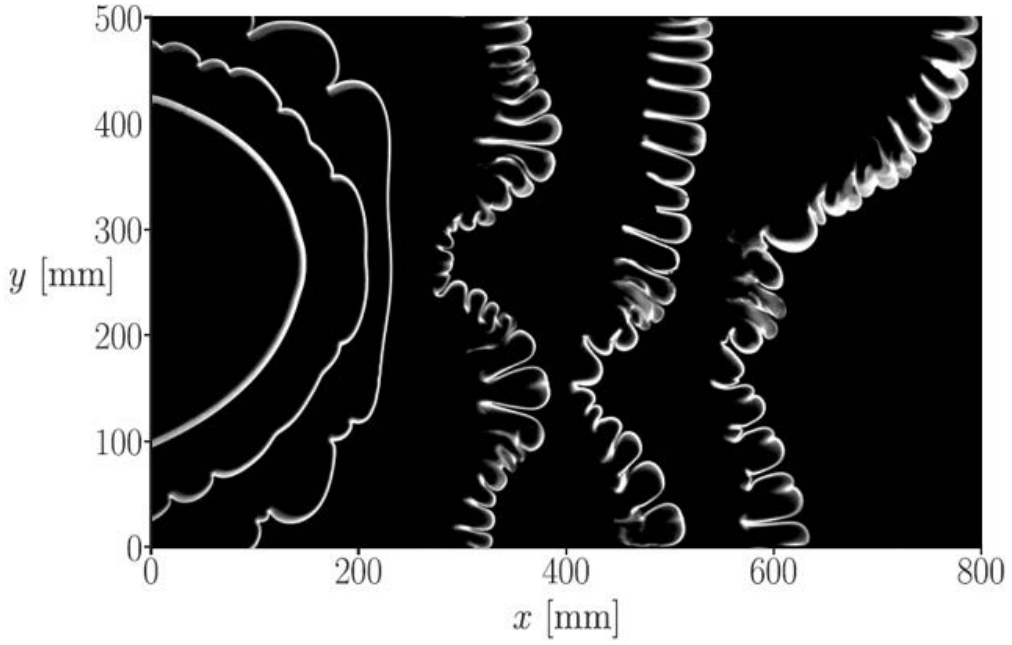

Figure 6.8: Flame front evolution propagating at $\phi = 1.2$.

Evidence of that is provided by Figures 6.9 and 6.10, where it is clearly visible the time it takes the flame to propagate throughout the cell, 2.23 seconds as compared to 0.89 s for the stoichiometric case or 1.03 s for the lean case. This is directly related to what it has been explained in Section 3.3, where Figure 3.4 shows this tendency of the flame speed affected by the adiabatic flame temperature to peak around $\phi = 1 \sim 1.1$ and decrease for leaner and richer mixtures.

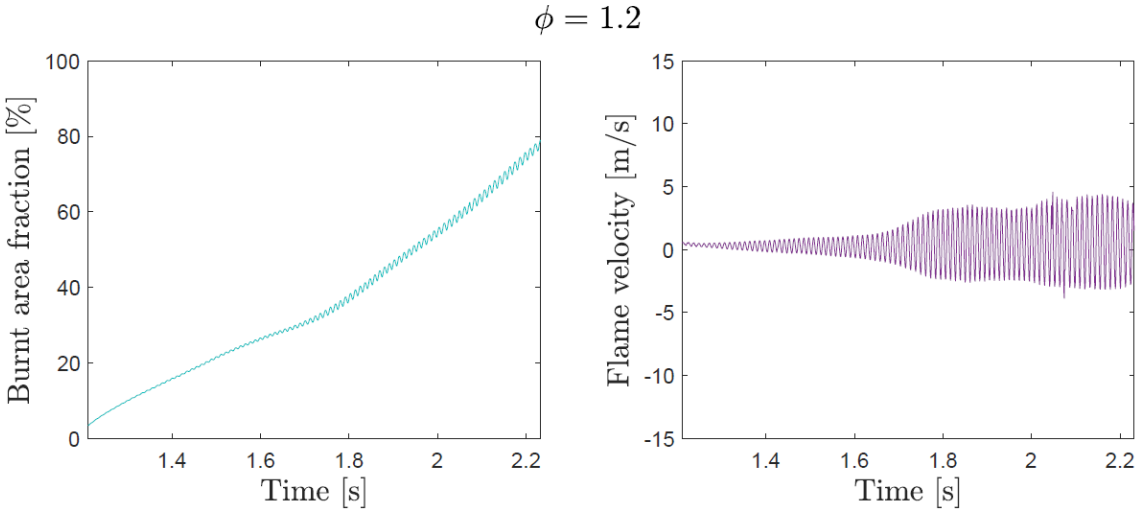

Figure 6.9: Plots obtained after image processing: burnt area fraction in percentage at the left, flame velocity at the right for the lean case ($\phi = 1.2$).

This can be ratified as well if reader compares the velocity plots. It can be noticed how the flame reaches a maximum velocity of 4.56 m/s, being the lowest one of the three cases, and thus, the least violent. Also, it has to be remarked the smooth profile it presents the rich flame velocity, which leads to an almost linear slope for the burnt area fraction rate (although oscillations do not disappear).

In this case, the moment at which the finger-like shape emerges is not so evident as before. Nevertheless, it can be estimated to turn up at $t_3 = 1.7$ s, a second later than in the other cases. However, from the left plot of Figure 6.9 and Figure 6.8 it can be perceived that although this instability appears later in time, it does not manifest in the half of the chamber as usual, but when it reaches about the 30% of it.

Finally Figure 6.10 represents the same profiles as before, but a little bit smoother, in accordance with the velocity one. It can be seen how the average values are smaller and how the acceleration in the vertical axis provoked by the compressed gases is practically half of the stoichiometric and lean cases, which only reaffirms what it has been said about the abruptness of the flame.

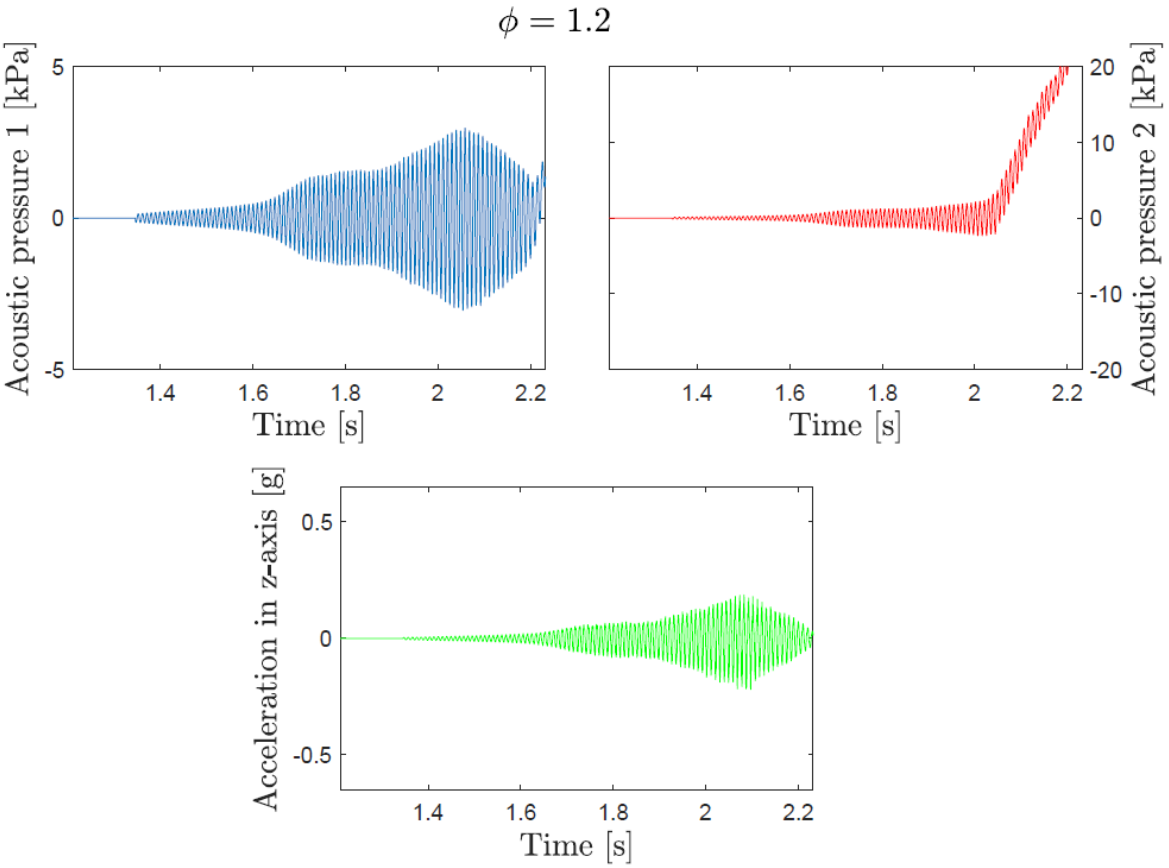

Figure 6.10: Data obtained from the sensors: acoustic pressure of sensor 1 and 2 at the top, respectively, and acceleration of the vertical component at the bottom for the lean case ($\phi = 1.2$).

In conclusion, the program can be validated as it has been proved that it works properly. Nonetheless, the results provided do not match with the ones proposed by F. Veiga et al in [20]. The main difference as compared to their study is the existence of a critical equivalence ratio which places the transition between oscillatory regimes, that is, a limit beyond which secondary instabilities do not appear. The value for this parameter was set to $\phi > \phi_c \approx 0.95 \pm 0.05$.

Figures 6.11a and 6.11b represent this phenomenon which clearly does not apply to the studied cases stated in this section as no evidence of such a critical value has been found. This is a clear consequence of the structural changes applied lately to the experiment (see Section 4.2).

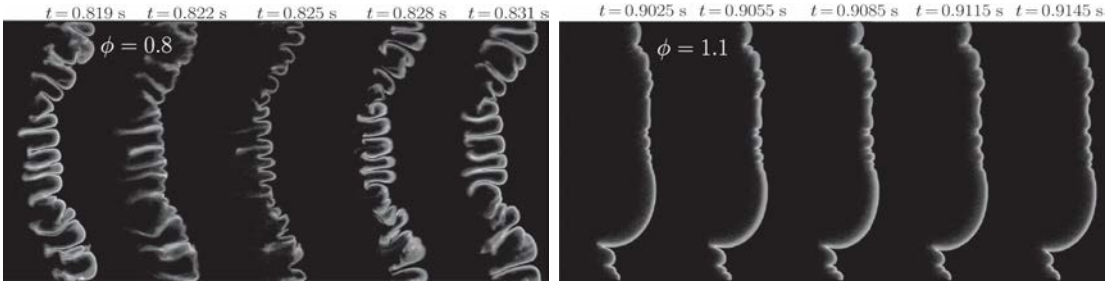

(a) (b)

Figure 6.11: Top view of a methane flame propagation during a short interval of time showing: **(a)** secondary instabilities ($\phi < \phi_c$), **(b)** primary instabilities only ($\phi > \phi_c$) [20].

7 Budget

The budget of this project is shown in Table 5 where all the components used in this experiment are detailed.

As it can be noticed, most of the costs (86%) come from the recording devices, that is, the high-motion camera, the DAQ, the accelerometer and the pressure sensors. Only the 10% of the cost represents the actual elements needed to carry a combustion without measuring anything (combustion chamber, ignition mechanism, filling and pneumatic system, gases, electronics and computer) and the remaining 4% depicts the labour of the engineer working for 300 hours, approximately.

Table 5: Project budget.

Systems	**Item**	**Cost [€]**
Combustion chamber	Aluminum structure	200
	Tempered glass	435
	Silicone gasket	30
	Methacrylate frame	70
	Clamping clips	300
Ignition mechanism	Glow plug	12
	Battery	100
	Temporizer	200
Filling system	Valves and tubes	50
	Fuel mass flow controller	2,300
	Air mass flow controller	900
	Pressure regulator (5 to 2 bar)	40
Pneumatic system	Actuators	350
Gases	Methane bottle and pressure regulator	400
Recording system	High-motion camera	70,000
	Computer	700
	DAQ, accelerometer and pressure sensors	10,000
Electronics	Arduino	15
	Cables, protoboard, relays	25
	Security box	40
Labour	Engineer salary (12€/hour)	3600
Computer programs licensing	LabVIEW License	3300
	MatLab Student License	Free
	Total	**93,067**

8 Conclusions and further work

The work performed in this project explained throughout this report has proved how the initial objectives have been successfully fulfilled and even improved going further.

As a response to the need to automate the experiment carried out by the Fluid mechanics group here at Universidad Carlos III de Madrid, a LabVIEW program has been worked out as well as the development of a validation process in order to attest its performance and right functioning.

Despite the aim of the project was to synchronize the camera and DAQ so as to obtain accurate results in order to perform a detailed study of the premixed flames, it has been possible not only to achieve this goal, but to implement in the code all the devices used in this experiment.

The direct impact of this point is that not only the delay between the videos and pressure data has disappeared, but also an improvement in security, reliability and amenity has been accomplished. The simple fact of having the control of all the components in the same location allows the user to perform the experiments with no failures as everything is settled and no manual action is required. Moreover, the use of actuators provides the project with more precision as no gas leaks can take place and more security since the user does not need to be right at the cell location, but he or she can control everything from the distance. Also, thanks to the automatization, the data obtained has more rigor as all the times the experiment is repeated, it is executed under the same conditions.

The program has been verified and validated by performing three experiments with three different equivalence ratios. It has been demonstrated how LabVIEW works with a real simulation and how its output files are treated during the post-processing with the objective of making conclusions. Both the videos and pressure data have given what expected.

Further work

Further work should be oriented mainly in enhancing the actual code, since there are no more devices taking part in the project to automate. One of the most urgent issue in which the student has been working on during the last weeks but with no apparent success, is the upgrading of the program to accept more than one fuel, that is, to add an extra fuel mass flow controller to study a premixed flame of a mixture diluted with Nitrogen or Helium, for example.

Looking to the future and to refine the security system, the code could be easily changed so the actuators opened and closed automatically and everything were even more automatic. For that purpose, the Hele-Shaw cell would need to be storage in a cubicle with protecting walls so there were no possibility of harm when they activated automatically.

Another task to work on, although not related to the automatization, is the study of how the structural changes carried out throughout the last months impact on the outcomes of the experiment. It has been noted how for the same equivalence ratio, the results differ from what it was studied at the beginning by F. Veiga. It has been proved that the values are shifted with respect to the ones of last year, but no conclusions have been reached yet.

References

[1] M. O. Bressano and A. S. Cortés, "Evolución histórica de la automatización de los procesos industriales."

[2] R. S. Alghni, *Methane gas: a renewable energy source*. PhD thesis, 2010.

[3] M. S. Sanz and E. A. F. Tarrazo, "Combustión eficiente de biocombustibles con aplicación a la generación portátil de potencia," tech. rep., 2015.

[4] M. to Markets, "La importancia del metano y las actividades de reducción de sus emisiones.." https://www.globalmethane.org, 2008.

[5] C. K. Law, *Combustion physics*. Cambridge ; New York: Cambridge University Press, 2006.

[6] S. D. Heister, W. E. Anderson, T. L. Pourpoint, and R. J. Cassady, *Rocket Propulsion*. Cambridge: Cambridge University Press, 2019.

[7] E. Hahn, "Combustion of propane vs incomplete combustion: Formulas and equations," 2018.

[8] "Combustion - definition, types of combustion, examples," 2018.

[9] T. Trindade, A. Ferreira, and E. Fernandes, "Characterization of combustion chemiluminescence: An image processing approach," 2014.

[10] G. Zizak, "Flame emission spectroscopy: Fundamentals and applications," 2002.

[11] N. Peters, *Combustion Theory*. Princeton: RWTH Aachen University, 2010.

[12] Y. Minamoto, "Bunsen flame — flowsquare." http://flowsquare.com/2013/12/16/bunsen-flame/, 2013.

[13] H. Pitsch, *Turbulent Non-Premixed Combustion*. Institut für Technische Verbrennung: CEFRC Combustion Summer School, 2014.

[14] *"Cool" Flame Pictures*. University of Toronto: Institute for Aerospace Studies.

[15] Ocelia, "Llama de fuego turbulenta 4k." https://sp.depositphotos.com/170422530/stock-video-turbulent-fire-flame-4k-start.html.

[16] T. W. Davies, "Fourier's law," *Thermopedia*, 2011.

[17] S. L. Jacques and S. A. Prahl, "Fick's 1st law of diffusion," 1998.

[18] R. B. Bird, *Transport phenomena*. New York: John Wiley Sons, 2nd ed., 2007.

[19] G. Joulin and T. Mitani, "Linear stability analysis of two-reactant flames," *Combustion and Flame*, vol. 40, pp. 235–246, 1981.

[20] F. Veiga-López, D. Martínez-Ruiz, E. Fernández-Tarrazo, and M. Sánchez-Sanz, "Experimental analysis of oscillatory premixed flames in a hele-shaw cell propagating towards a closed end," *Combustion and Flame*, vol. 201, pp. 1–11, 2019.

[21] D. Fernández-Galisteo, V. N. Kurdyumov, and P. D. Ronney, "Analysis of premixed flame propagation between two closely-spaced parallel plates," *Combustion and Flame*, vol. 190, pp. 133–145, 2018.

[22] S. H. Yoon, T. J. Noh, and O. Fujita, "Effects of lewis number on generation of primary acoustic instability in downward-propagating flames," *Proceedings of the Combustion Institute*, vol. 36, no. 1, pp. 1603–1611, 2017.

[23] A. L. Sánchez and J. Rodríguez-Rodríguez, *Fluid Mechanics: an Introduction and some Relevant Applications*. Universidad Carlos III de Madrid: Fluid Mechanics Group, 2011.

[24] X. Bai, "Lecture 4: Transport of mass, momentum and heat," 2015.

[25] J. D. A. Jr, *Governing Equations of Fluid Dynamics*, pp. 15–51. Computational Fluid Dynamics, Berlin, Heidelberg: Springer, 2009.

[26] T. Ogawa, V. N. Gamezo, and E. S. Oran, "Flame acceleration and transition to detonation in an array of square obstacles," *Journal of Loss Prevention in the Process Industries*, vol. 26, no. 2, pp. 355–362, 2013.

[27] P. Clavin, "Premixed combustion and gasdynamics," *Annual Review of Fluid Mechanics*, vol. 26, no. 1, pp. 321–352, 1994.

[28] V. V. Bychkov and M. A. Liberman, "Dynamics and stability of premixed flames," *Physics Reports*, vol. 325, no. 4, pp. 115–237, 2000.

[29] P. Clavin and G. Searby, *Combustion Waves and Fronts in Flows: Flames, Shocks, Detonations, Ablation Fronts and Explosion of Stars*. Cambridge: Cambridge University Press, 2016.

[30] P. G. Athul, *Stability of Laminar Premixed Flames*. Chennai, India: Indian Institute of Technology, 2015.

[31] F. A. Williams, *Combustion theory : the fundamental theory of chemically reacting flow systems*. Boca Raton (Florida): CRC, 2nd ed., 2018.

[32] M. Matalon, "Intrinsic flame instabilities in premixed and nonpremixed combustion," *Annual Review of Fluid Mechanics*, vol. 39, no. 1, pp. 163–191, 2007.

[33] G. Searby, "Acoustic instability in premixed flames," *Combustion Science and Technology*, vol. 81, no. 4-6, pp. 221–231, 1992.

[34] C. V. Silva, *Estudio experimental de llamas de premezcla de DME en una celda Hele-Shaw*. Leganés: Universidad Carlos III de Madrid, 2018. Trabajo de fin

de grado.

[35] A. G. Gala, *Experimental study of the effect of nitrogen dilution on premixed propane-air flames propagating in a hele-shaw cell*. Leganés: Universidad Carlos III de Madrid, 2018. Trabajo de fin de grado.

[36] Bosch, "Glow plugs." https://nl.bosch-automotive.com.

[37] "National instruments website." https://zone.ni.com, 2017.

Appendix A: User's guide

This guide is intended to help users to better understand the procedure to be followed for a correct functioning of the LabVIEW program developed in this project.

1. Make sure all the devices are well connected to the computer and the COM ports are the following ones: COM8 for Arduino and COM2 for the fuel mass flow controller.
2. Open the folder called "Flame propagation program" and run the executable "Flame propagation".
3. To stop the program at any time, close the main tab. The "Stop Program" button only works if the DAQ is not connected.
4. In the "Connection" tab, verify that the IP Address of the DAQ is 172.21.80.21 and its port is 139.
5. Click on "Connect" to establish the connection between the DAQ and the computer. It may give an error if it is the first time we connect it. It can be solved by clicking again on "Connect" (a green light should appear if it is successfully paired).
6. To connect the camera, click on "Find Camera" and afterwards on "Connect camera".
7. If the Arduino has not suffered any change, the pins should remain with their default values.
8. If the user wants to see the live image of the camera, go to the "Gas" tab, click on "View" and "Live Start". In case the user wants to stop the live image, just click on "Live Stop".
9. Regarding the gas settings, the user can choose the type of gas and its units from the drop-down menu. The air flow is typically set to 2.4 SLPM (however the value to be introduced as a setpoint is 0.475 V_{DC}), but the user can change it introducing a value between 0 and 1 (being 1 equivalent to 5 SLPM and 0 equivalent to 0 SLPM). The fuel setpoint value can be changed accordingly to the desired equivalence ratio.
10. Before starting the gas filling, the user should go to the third tab "Obtain data" and set the recording time he or she wants for the obtention of data from the sensors, the delay between the glow plug is ignited and the camera starts recording and the most important one, to click on "Arm Camera" in order to prepare the camera for recording. The route where the DAQ file is stored can also be modified at this point.

11. In order to start the filling, close the Actuator 1 by clicking on “Connect”, set the filling time to 2-3 minutes, set the valve state to “On” and start the timer.
12. During the filling time the user will not be able to do anything else until the countdown comes to zero. At that instance, the red circle will turn into green and a voice message will sound telling the user the filling is complete and the actuators sequence he or she should follow.
13. Once everything is ready, push the green button to ignite the flame and start the ignition.
14. After the ignition is over, leave the cell ready for cleaning (close actuator 1 and open actuator 2). In the “Obtain data” tab, set the purge timer to 1 minute and click on “Start” in order to clean the cell with fresh air.
15. The user can take a look at the pressure and acceleration graphs in order to see if the experiment is as expected or not (notice the horizontal scroll bar at the bottom right to watch the left part of the graphs). It is also possible to watch the video by clicking on “Play Video” in the “Obtain Data” tab and stop it by clicking on “Stop Video”.
16. If the user wants to run another experiment, the air and fuel setpoints should be checked since they turn to zero once the gas filling is over. (Repeat steps 8-15)
17. If no more experiments are going to be run, open both Actuators for security reasons and close the program by clicking on the “X” of the main tab.

Appendix B: Electronic circuit

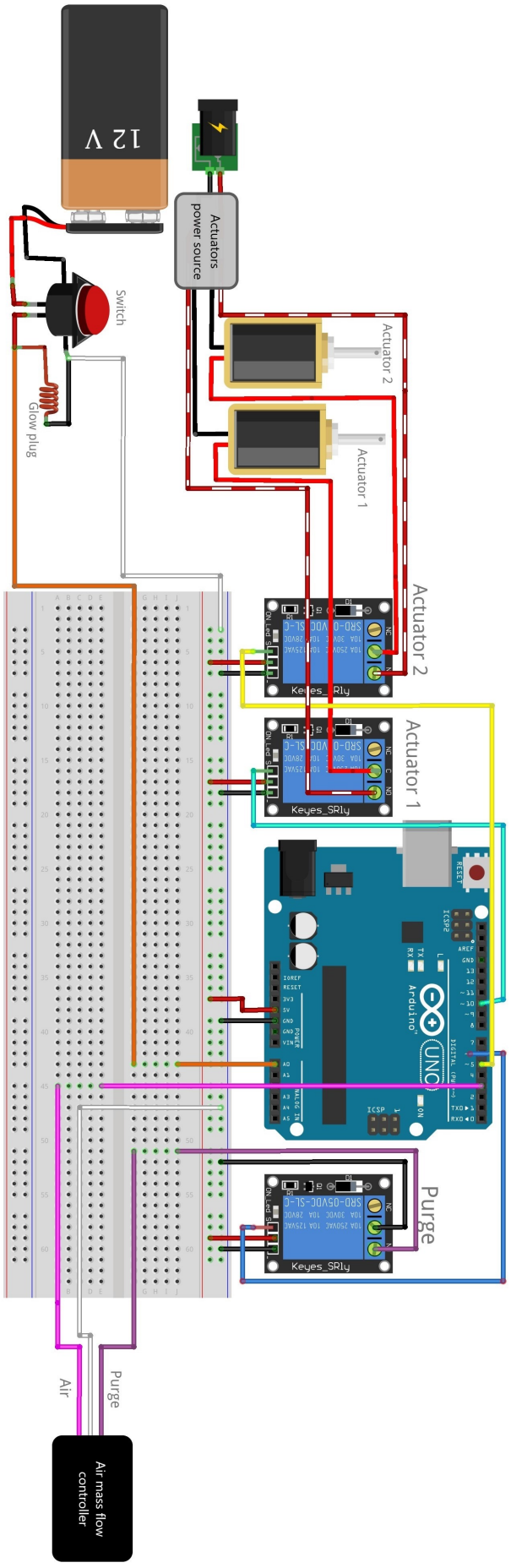

Appendix C: LabVIEW code - Block diagram

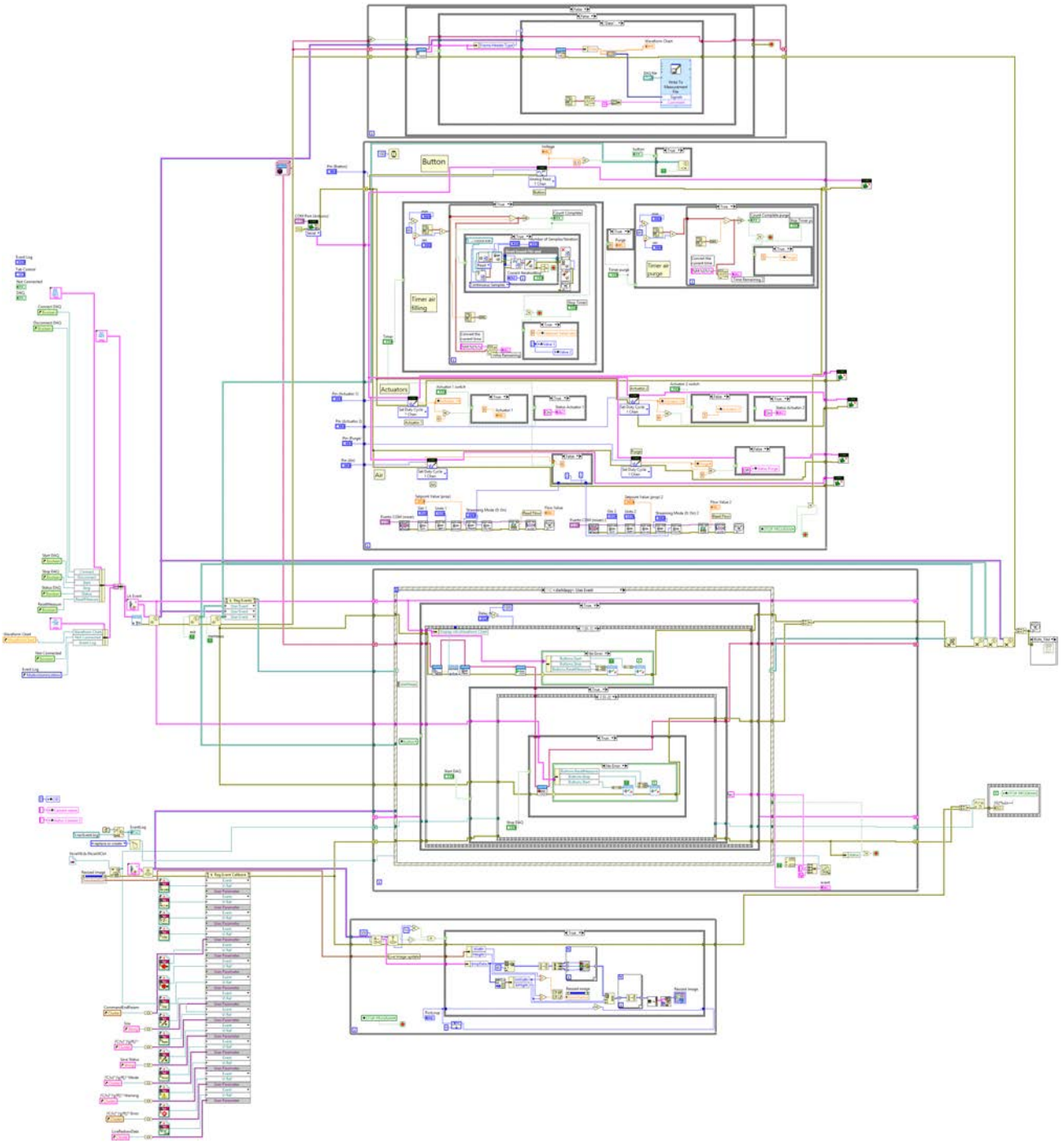

Appendix D: MatLab code - Image processing

```
%%%%%%%%%%%%%%%%%%%%%%%%%%%%%%%%%%%%%%%%%%%%%%%%%%%%%%%%%%%%%
%%%%%%%%%%%%%%%%%% VIDEO PROCESSOR %%%%%%%%%%%%%%%%%%%%%%%%%%%
%%%%%%%%%%%%%%%%%%%%%%%%% F. Veiga %%%%%%%%%%%%%%%%%%%%%%%%%%%
%%%%%%%%%%%%%%%%%%%%%%%%%%%%%%%%%%%%%%%%%%%%%%%%%%%%%%%%%%%%%


%% Input Parameters
video         =    VideoReader('08_tocado.avi');  % Reading the video.
startframe    =    20;
endframe      =    675;
n             =    (endframe - startframe);
se            =    strel('disk',5);

%% Processing the video
background    =    read(video,1);
movie_all     =    read(video,[startframe,endframe]);
movie         =    movie_all - background;

%% Obtaining the contours.
for i = 1:n
    % Image processing.
    frame      =    movie(:,:,1,i)';
    threshold  =    graythresh(frame);
    bwframe    =    imbinarize(frame,0.2);
    bwframe    =    imdilate(bwframe, se);
    bwframe    =    bwareafilt(bwframe,1);

    % Contours.
    [Prow, Pcol]    =    find(bwframe,1);
    cont            =    bwtraceboundary(bwframe,[Prow Pcol],'W');
    [Plrow, Plcol]  =    find(bwframe,1,'last');
    index           =    find(cont(:,1) == Plrow & cont(:,2) == Plcol);
    extcont         =    cont(1:index,:);
    intcont         =    cont(index:end,:);

    extcontours{i,1} =   [extcont(:,2) extcont(:,1)];
    intcontours{i,1} =   [intcont(:,2) intcont(:,1)];
end

% Saving the data.
save('external_cont.mat', 'extcontours');
save('internal_cont.mat', 'intcontours');
% Check the last frame.
figure(); imshow(frame); hold on;
plot(intcont(:,2), intcont(:,1), 'b.');
plot(extcont(:,2), extcont(:,1), 'r.')
```

Appendix E: MatLab code - Area and velocity calculation

```
                %%%%%%%%% ANALYSIS OF THE FLAME FRONT %%%%%%%%%
                    %%%%%%%%%%%%%%% By fVe1ga %%%%%%%%%%%%%%%%%%

%% Input.
file            =   'external_cont.mat';
listing         =   load(file);
listing         =   listing.extcontours;
n_im            =   numel(listing);
file_number     =   1:n_im;

video           =   VideoReader('08_tocado.avi');  % Reading the video.
background      =   read(video,1)';                % Getting background
    of the video.
%% Calculate.
time_step       =   1; %In ms.
time            =   linspace(0, n_im*time_step, n_im)';
[ypix, xpix]    =   size(background(:,:,1));
xres            =   500./xpix;
yres            =   800./ypix;

Area            =   zeros(n_im,1);
%% Loop.
for i = 1:n_im
    % Reading data.
    coords      =   listing{i,1};
    x           =   coords(:,1)*xres;
    y           =   (ypix - coords(:,2))*yres;

    % Creating the arc-length parameter.
    t           =   (cumsum(sqrt([0,diff(x)'].^2 + [0,diff(y)'].^2)))';

    area        =   trapz(x,y);

    Area(i)     =   area;
end

Area            =   Area./(500*800);
vel                 =   gradient(Area.')*500./gradient(time).'; %m/s
```